Research Article

Optimization of Low-Carbon Footprint Quaternary and Quinary (37% Fly Ash) Cementitious Nanocomposites with Polycarboxylate or Aqueous Nanosilica Particles

Styliani Papatzani [1,2] and Kevin Paine[1]

[1]*BRE Centre for Innovative Construction Materials, University of Bath, BA2 7AY Bath, UK*
[2]*Hellenic Ministry of Culture, Directorate of Restoration of Medieval & Post-Medieval Monuments, Tzireon 8-10, 11742 Athens, Greece*

Correspondence should be addressed to Styliani Papatzani; spapatzani@gmail.com

The dispersion medium of nano-SiO_2 (nS) particles can have a significant effect on the properties of nanoparticles themselves and consequently on the cement binders it will be added to. In this paper, nS particles dispersed in (a) polycarboxylate or (b) water were added to a low-carbon footprint reference binder containing 43% Portland cement (PC), 20% limestone powder (LS), and 37% fly ash (FA) by mass of binder. Eight quaternary binders containing nS, PC, LS, and FA and eight quinary binders comprising nS, PC, LS, FA, and silica fume (μS) were investigated. nS was added at 0.1%, 0.2%, 0.5%, or 1.0% by mass of binder as a replacement of LS for the quaternary binders and at 0.5% or 1.0% for the quinary binders. The nanoparticles were examined via transmission and X-ray scanning electron microscopy (TEM/SEM/EDX). For the pastes, compressive strength tests and thermal gravimetric analyses (TGAs) were performed at days 1, 7, 28, and 56, all testified to additional pozzolanic activity and additional C–S–H production. X-ray diffraction analyses and backscattered scanning electron imaging carried out on specific formulations also confirmed this finding at days 1, 28, and 56. Notwithstanding the additional pozzolanic reactivity, nS particles could not mitigate the delayed hydration of the reference paste in the early ages. In such complex formulations, the hydration products seem to create a wrapping around the FA particles delaying their activation at early ages. At later ages, the 0.5% nS addition provided strength, microstructural, and hydration improvements. The polycarboxylate/nS particles provided more pronounced strength improvements at 0.5% addition, possibly due to their superplasticizing effect. Lastly, a tabulated literature review on the thermal decomposition ranges of the hydration products of cementitious nanocomposites is also presented.

1. Introduction

For the production of cement, carbon dioxide is emitted in two ways; as a product of the burning process of fossil fuels and as a product of the chemical conversion of limestone to lime. This process is responsible for about 8% of the total manmade CO_2 emissions worldwide. For this reason, the cement industry in particular has invested significant effort in reducing the CO_2 impact of cement production over the past decades. The European Cement Association has distinguished four key areas for producing low-carbon footprint cement;

(i) Lowering the clinker content and increasing the supplementary cementitious materials (SCM) content

(ii) Producing novel cements

(iii) Modernizing existing cement plants with energy efficient technologies, products, and processes and making use of alternative fuels such as biomass or waste materials for the clinkering process

(iv) Capturing CO_2 and reusing it in the production process

At the same time, the Eurocodes are currently providing the upper and lower limits of cement substitution and SCM addition [1]. In fact, for CEMII/A-L (binary) cements, the permissible clinker content lies within 80–95% by mass of binder and the allowable limestone content is restricted to

6–20%. As for the Portland-composite cements, i.e. cements that contain both fly ash and limestone at a total maximum of 35%, the allowable amount of clinker must not be less than 65% according to the Eurocodes. Any other combination beyond these restrictions can potentially incur a series of issues, such as prolonged setting times, reduced compressive strengths, and nonhomogeneous microstructure.

Nanotechnology through a number of applications has entered in our lives. Construction materials were amongst the first sectors that benefited through the use of nanosized particles (at least one dimension below 100 nm) and their observation at the nanometric scale, close to the molecular level. In the past five years, extensive research has yielded results on the development of nanocomposites suitable for building materials. In recent research, results on the investigations of the limits of the clinker reduction and the SCM are studied. The need to produce low-carbon footprint cements has driven scientists to reduce the greatest contributor in CO_2 emissions, clinker, to unprecedented levels, beyond permissible limits described by codes. In recent research, results on the investigations of the limits of the clinker reduction and the SCM addition have suggested that the optimal replacement level in binary and composite limestone cement is 15%. In fact, binary systems containing Portland cement (PC) at 85% and LS at 15% were freeze-thaw durable, whereas the PC, fly ash (FA), and LS systems prolonged the initial setting time of all concretes tested and reduced early age strength but required less superplasticizer compared with the PC mix [2]. Ternary and quaternary cements can be optimized for additional durability, since the compositions tested improved the resistance to chloride ingress, although carbonation is yet to be encountered with, and it was overall postulated that these composite formulations can significantly decrease the CO_2 footprint.

Apart from the effort to increase the LS content in the formulations, many research teams have been focused on the exploration of the upper bounds of FA addition, particularly because FA is a by-product from combustion of coal, primarily from coal-fired power plants. Although FA in the UK and other countries might be in shortage [3], there is an urgent need to increase the use of fly ash (FA) in the US and worldwide. For this, researchers have attempted to reduce Portland cement (PC) proportions and increase FA proportions up to 50%. However, as summed up in a recent review paper, the typical optimal amount of FA substitution for general purpose concretes is limited to 30%, whereas FA substitution up to 50% has been used for mass concreting in foundations and dams [4], as it reduces setting and shrinkage cracking. The beneficial effects of the additional C–S–H produced and the consistence and microstructural enhancement observed are counteracted by the early-age strength reduction at high FA substitutions and the many unreacted FA particles even after 90 days. It is postulated, though, that the adverse effects can be counteracted with the addition of nanoparticles [4]. In a recent project report, the reference paste contained 70% PC and 30% FA to which 0.5% of nanolimestone or nanosilica (nS) or nanoclay was added at a water-to-cement ratio equal to

0.5 [5]. In this research, pozzolanic studies of 20 g $Ca(OH)_2$ plus 5 g silica fume was compared to 20 g $Ca(OH)_2$ plus 5 g nanosilica concluding that after 7 days of hydration the pozzolanic reaction of nS was almost complete, due to the unsaturated Si–O bonds on the surface of the particles. With time, however the effect of nS is similar to that of silica fume.

Furthermore, a recent review on the effects of nS and FA in cement paste, mortar, and concrete formulations shows that, by 2014, only 6 papers have been published in ternary blends investigating consistency, ammonium chloride resistance, and compressive and flexural strength [6].

Others studies led by the authors of the present paper suggest that cementitious composite pastes and mortars comprising of 60% PC and 40% LS can be further enhanced by the addition of just 0.5% nS by total mass of solids in terms of mechanical strength and additional hydration reactions [7–9]. Moreover, it was found that cementitious composite pastes and mortars containing 60% PC, 20% FA, and 20% LS can be further enhanced by the addition of just 0.5% nS by total mass of solids [10]. In this publication, strength gain was linked to $Ca(OH)_2$ consumption towards the production of additional C–S–H in a single graph, which can assist in future formulation design.

With the present paper, the first two key areas identified by the European Cement Association are simultaneously addressed. In an effort to further optimize cementitious nanocomposites towards the development of a low-carbon footprint cement formulation, in this paper, a very low PC content (43% by total mass of solids) and a high supplementary cementitious material content (LS, FA, and silica fume summing up to 57% by total mass of solids) formulation was investigated. These proportions are far from the permissible, according to the European Standards, which state that in Portland-composite cements (i.e., cements that contain both FA and LS), the allowable amount of clinker should be at least 65% [1], as graphically shown in Figure 1. The PC content was reduced in favour of the FA content, lowering the PC/FA ratio to 1.16. In such composite cements, antagonism amongst the pozzolanic particles (FA, silica fume, and nS) is expected, and the extent of the phenomenon was assessed. Agglomeration of the nanoparticles was one of the possible limitations [11], and for this, two different nS dispersions were compared: an aqueous and a polycarboxylate-based one. Given recent results on the combined effect of polycarboxylate superplasticizers and nanosilica in binary (PC-nS) pastes, claiming the reduction in nS reactivity with immediate mixing [12], in this research, the combined effect of polycarboxylate nS in quaternary and quinary formulations has been investigated and further clarified. To the best knowledge of the authors, this is the first study presented on quaternary and quinary low-carbon cementitious nanocomposites against a number of parameters; hydration and pozzolanic reactions, strength development, microstructural enhancement, and comparison of all the above with two different types of nanosilica particles.

Apart from compressive strength tests and scanning electron imaging, extensive thermal gravimetric analysis

FIGURE 1: Permissible and nonpermissible limits of clinker substitution/SCM addition according to EN 197-1 and the challenge of the current research.

(TGA) was required in order to attest the consumption of the $Ca(OH)_2$ towards the production of additional C–S–H.

TGA is the technique by which the mass change of a sample is monitored as a function of temperature change. A typical analysis comprises of heating up a sample from room temperature to 1000°C at a rate of 10°C/min. Three phases are distinguished: (i) the dehydration of C–S–H, ettringite, and monosulfate occurring approximately between 100°C and 180°C; (ii) the dehydration of $Ca(OH)_2$ taking place approximately between 400°C and 500°C; and (iii) the decomposition of $CaCO_3$ between 600°C and 800°C. The technique is offering an approximation of the C–S–H produced, the $Ca(OH)_2$ consumed, the extent of pozzolanic reaction, and evidence of carbonation of the samples [7, 10, 13–15]. The temperature ranges were selected after a further search in the literature, from which a tabulated literature review on TGA was also developed. Although there is a significant amount of papers in which TGA results are presented, thermal gravimetric tests in binders containing nanoparticles are limited. In essence, due to the addition of nanoparticles, the bond strength is diversified and hence temperature decomposition shifts are expected. It was, therefore, essential to conduct a literature review on the thermal decomposition stages, given by other researchers in order to ascertain the abovementioned temperature ranges and distinguish the hydrates decomposing at the increasing temperature intervals (Table 1).

2. Materials and Methods

2.1. Materials. The materials used were as follows:

(i) Portland limestone cement CEMII/A-L42.5, with a limestone content of 14%, conforming to EN 197-1. The supplier gave the following clinker composition: 70% C_3S, 4% C_2S, 9% C_3A, and 12% C_4AF. In mix proportioning, the Portland cement (PC) content (86% by mass) was considered separately from the limestone (LS) content (14% by mass).

(ii) Limestone (additional LS), conforming to EN 197-1. The total LS content of each paste was the sum of that contained in the Portland limestone cement and this additional LS.

(iii) Fly ash (FA), conforming to EN 450. The oxide composition provided by the material data sheet was 53.5% SiO_2, 34.3% Al_2O_3, 3.6% Fe_2O_3, and 4.4% CaO.

(iv) Silica fume (μS), in undensified dry form, conforming to BS EN 13263. According to the material data sheet: specific surface area = 15–30 m^2/g; mean particle size = 0.15 μm.

(v) Commercially available amorphous nS 15% by mass of nanoparticles in a polycarboxylate suspension (GnS) (Figure 2).

(vi) Commercially available colloidal amorphous nS 15% by mass of nanoparticles in an aqueous suspension (LnS) (Figure 2).

2.2. Methods

2.2.1. Formulation of Quaternary Cementitious Nanocomposite Binders. A series of composite cement binders was designed having PC43LS20FA37 (43% Portland cement, 20% limestone, and 37% fly ash by total mass of binder) as a reference paste. The water to binder (w/b) ratio was kept constant at 0.3 (Table 2). These pastes were designed with a high content of FA, which permitted an investigation into possible effects of pozzolanic interference between the two different types of nS and other pozzolanic materials. The PC content was kept constant, and the content of nS solids was deducted from the LS content. This was done in order to keep the $Ca(OH)_2$ production during PC hydration comparable in all pastes, so as to detect possible pozzolanic reactivity of the nanoparticles in composite cement formulations. The general formula of the

Table 1: TG decomposition temperatures of hydration products of cementitious nanocomposite binders and major conclusions.

Binder analyzed	Purpose of TGA	Sample preparation/gas used/ sample weight and heating rate	Temperature intervals	Results and comments	Reference
PC60FA40 PC57.5FA40 + 2.5nS PC55FA40 + 5.5nS Mortars @w/b = 0.5	Measure pozzolanic activity in terms of Ca(OH)$_2$ content	Samples were oven dried @105°C for 4 h Atmospheric pressure About 20 mg 15°C/min	Weight loss between 440 and 510°C due to decomposition of Ca(OH)$_2$	OPC + type F FA + colloidal nS of 20 nm and 10 nm average particle size. Depletion of Ca(OH)$_2$ at high FA and nS content pastes, cured in water at 70°C for 7 days, did not allow further hydration of FA. In general decrease in hydration degree of FA at later ages due to the low Ca(OH)$_2$ content.	[16]
20 g of Ca(OH)$_2$ content + 5 g of colloidal nS compared with 20 g of Ca(OH)$_2$ content + 5 g of μS at both @w/b = 2	Ca(OH)$_2$ content at different ages	Limewater curing Hydration arrested with acetone and oven – dried at 105°C for 4 h	@440–510°C: decomposition of Ca(OH)$_2$	Ca(OH)$_2$ contents were calculated on the ignited basis at 950°C for 30 min Pozzolanic reaction of nS was completed by day 7, however, for μS, over one month was needed.	[17]
1%, 2%, and 3% halloysite nanoclay by mass replacement of CEMI in mortar 95% CEMI-32.5 + 5% μS + 2% SP @w/b = 0.45—limewater curing	Measure Ca(OH)$_2$ consumption	Not mentioned (n/m)	Peaks @105–120: decomposition of C-S-H @105–120: decomposition of gehlenite hydrate (C$_2$SAH$_6$) @295–320: decomposition of hydrogarnet (C$_3$SAH$_6$) @480–490°C: dehydroxylation of Ca(OH)$_2$	Differential scanning calorimetry (DSC) at 28 days showed consumption of Ca(OH)$_2$ towards formation of C–S–H.	[18]
OPC + 0.5%, 1%, 1.5% and 2% nS by mass replacement of OPC in mortar	Measure pozzolanic activity	Saturated LS curing for 28 d. Then in water until day 90. N$_2$ 4°C/min, from 100 to 650°C	n/m	The loss in weight of the specimens is increased by increasing the nanocontent in concretes, maybe due to more formation of hydrated C–S–H gel.	[19]
5% nS by mass replacement of OPC mix, 7- and 28-day old	Hydration of OPC paste and 5% nS paste	n/m From 20 to 1000°C	@120–190°C: evaporation of capillary water, decomposition of C-S-H @450–500°C: dehydroxylation of Ca(OH)$_2$ @700–780°C: Decarboxylation of CaCO$_3$	Increased hydration with use of nS.	[20]

TABLE 1: Continued.

Binder analyzed	Purpose of TGA	Sample preparation/gas used/ sample weight and heating rate	Temperature intervals	Results and comments	Reference
5% nS by mass replacement of OPC	Study of decomposition of hydration products	n/m N_2 10°C/min 20–1000°C-held @105°C for 2 hours to remove free water	@20–105°C: loss of free water and decomposition of ettringite @105–400°C: gradual mass loss due to dehydration of C–S–H and loss of interlayer, absorbed and chemically bound water @450°C: dehydroxylation of $Ca(OH)_2$	Reduction in amount of $Ca(OH)_2$ in sample with nS shows evidence of pozzolanic reaction.	[21]
1, 2, 3, 4, and 5% nS by mass replacement of OPC + 1% SP @w/ b = 0.4 nS was dispersed in the SP	Study of decomposition of hydration products	n/m N_2 4°C/min From 110 to 650°C	110–650°C: dehydration of hydrated products	Powder 99.9% pure nS of 15 nm average particle size After 28 days of curing, mass loss of samples increased with increasing nS content up to 4% by mass SP: polycarboxylate with condensate defoamer base admixture.	[22]
CEMI-52.5R + SP1.2 PC80μS20 + SP1.2 PC96.5nS3.5 + SP3 PC87.8μS12.2 + SP1.2 PC87.8μS10.2nS2 + SP1.2 All @w/b = 0.35 SP: carboxylic acid nS: 30% solids by mass	To study the effect of μS and nS and their combined use	Water curing at 21°C for 7, 28, and 90 days, samples with w/b ratio of 0.35 N_2 From 27 to 1000°C. 10°C/min	@~100°C: evaporation of water @115–125°C: partial dehydration of C–S–H @120–130°C: partial dehydration of aft @180–200°C: partial dehydration of AFm @450–550°C: dehydration of $Ca(OH)_2$ @~800°C: decarboxylation of $CaCO_3$	For 7 and 28 days (up to 400°C), samples with 3.5% nS and 2 + 10.2% nS + μS showed a higher weight loss when compared to 0% nS and 0 + 12.2% nS + μS, while for 20% μS, it was lower than that of 0% μS.	[23]
2%, 4%, 6%, and 8% nanometakaolin (NMK) by mass replacement of CEM-I mortars @w/b = 0.5	To study the effect of NMK	20°C/min N_2	Peaks @105–110°C: decomposition of C–S–H @160°C: decomposition of gehlenite @350°C: decomposition of hydrogarnet @470°C: dehydroxylation of $Ca(OH)_2$ @580°C: phase change of quartz going from alpha level to beta level	DSC analyses: the addition of NMP led to the consumption of $Ca(OH)_2$ and its transformation from well crystalline to ill-crystalline phases.	[24]

TABLE 1: Continued.

Binder analyzed	Purpose of TGA	Sample preparation/gas used/ sample weight and heating rate	Temperature intervals	Results and comments	Reference
0.2%, 0.4%, 0.6%, and 0.8% OMMT by mass replacement of ASTM-I PC @w/b = 0.55	n/m	n/m up to 1400°C	Peaks @100°C: capillary water evaporates @470°C: dehydroxylation of $Ca(OH)_2$ @720°C: decarboxylation of $CaCO_3$ @1300°C: glass transition temperature transforming the cement from powder into a melted material.		[25]
0%, 0.5%, and 2% of OMMT nC by mass replacement of type I PC mortars @w/b = 0.4, 0.485, and 0.55	Verification of organomodification of OMMT	n/m	@150°C: partial dehydration of C–S–H @300–400°C: The organomodifier decomposed	Verification of organomodification of clay particles.	[26]
CEM I 52.5R with polycarboxylic ether-based superplasticizer + limestone and quartz powder + sandstone and sand + 13 mm steel fibres 1, 2, 3, 4, and 5% nS	Effect of nS on ultra-high-performance concrete	Curing for 28 days hardened samples ground to powder and tested at 10°C/min	Peaks @105°C: capillary water evaporates @450°C: dehydroxylation of $Ca(OH)_2$ @800°C: decarboxylation of $CaCO_3$	The addition of superplasticizer retarded the dormant period of cement hydration. This effect is compensated by the addition of nS as age progresses.	[27]
Cement was replaced by FA and nS. The dosages of nS varied from 0% to 1%, 3%, and 5% by mass of the cementitious materials. The w/b and sand-binder ratios were 0.2 and 1.2, respectively	Effect of nS on ultra-high-performance cementitious composites	Samples were soaked in alcohol for 48h to arrest hydration and then milled to 80lm sieve particles, and then were subsequently dried, sealed, and tested at 7 days under TGA	Peak @110°C: capillary water evaporates @135–150°C: decomposition of C–S–H @400–500°C: dehydroxylation of $Ca(OH)_2$ @710°C: decarboxylation of $CaCO_3$ @800–910°C: curve bending towards exothermic reactions can be related to the transformation of some C_2S from a ^0_H crystallographic form to a ^0_L crystallographic form @1210°C: endothermic peak may be induced by the transformation of some C_2S from a ^0_H crystallographic form to a crystallographic form.	Pozzolanic and filler effects of nS were confirmed. Above 3% of nS addition serious agglomeration occurred.	[28]

TABLE 1: Continued.

Binder analyzed	Purpose of TGA	Sample preparation/gas used/sample weight and heating rate	Temperature intervals	Results and comments	Reference
CEM I 42.5R concrete + commercial nS suspension (10% solids by weight of water with nominal mean particle size of 20 nm) @0, 0.5, 1, and 1.5% replacement	Effect of nS and different w/b ratios on binary concretes	Approximately 100 mg of ground fragments of concrete with w/b = 0.65 at 1.5% nS substitution was analyzed under N_2 flow of 50 mL/min. Temperature 25°C up to 900°C @ a rate of 10°C/min temperature was held at 105°C for 2 hours to promote evaporation of free water.	@420–510°C: dehydroxylation of $Ca(OH)_2$ @720–810°C: decarboxylation of $CaCO_3$ and dolomite weight loss	The amount of CH consumed was estimated. Strength gain at higher nS additions is directly related to the w/b ratio.	[29]
Tricalcium silicate (C_3S) was prepared in the laboratory using an electric furnace at an elevated temperature of 1500°C powder nS was added at 1, 3, 5, and 10% with w/b = 0.4	Determination of CH and C-S-H content in hydrated C_3S paste	Heating rate of 5°C/min under nitrogen flow	400–500°C is due to the dehydration of CH; 600–800°C is because of the decarbonation of $CaCO_3$ The remaining mass loss between 105 and 1000°C is considered as the dehydration of C-S-H	Maximum nucleation effect of nS at 8h, when the rate of product C-S-H formation was higher than the control (~66% additional C-S-H and ~61% more CH with 10% nS addition) At 24h of hydration, ~25% additional C-S-H was formed and CH content reduced by ~32% with 10% addition showing the pozzolanic effect of nS.	[30]
PC 40%, LS 20%, and FA 20% by mass of binder and nS as PC replacement	Determination of CH and C-S-H content in hydrated paste	Heating rate of 10°C/min under nitrogen flow up to 1000°C	@105–180°C: decomposition of C-S-H, ettringite, and gehlenite @185–200°C and 270–380°C: monosulfate of @440–510°C: dehydroxylation of $Ca(OH)_2$ @700–810°C: decomposition of $CaCO_3$	Increase in the $Ca(OH)_2$ towards the production of additional $CaCO_3$ directly correlated with compressive strength increase.	[10]
PC 60% and LS 40% by mass of binder and nS as PC replacement	Determination of CH and C-S-H content in hydrated paste	Heating rate of 10°C/min under nitrogen flow up to 1000°C	@105–180°C: decomposition of C-S-H, ettringite, and gehlenite @440–510°C: dehydroxylation of $Ca(OH)_2$ @700–810°C: decomposition of $CaCO_3$	Consumption of $Ca(OH)_2$ towards the production of additional C-S-H directly correlated with compressive strength increase.	[7–9, 31]
PC 60%, LS 40% by mass of binder and 1% nano-montmorillonite as PC replacement	Determination of C-S-H content in hydrated paste	Heating rate of 10°C/min under nitrogen flow up to 1000°C	@105–180°C: decomposition of C-S-H, ettringite and gehlenite	Production of additional C-S-H	[32]

TABLE 1: Continued.

| Binder analyzed	Purpose of TGA	Sample preparation/gas used/ sample weight and heating rate	Temperature intervals	Results and comments	Reference
50% lime putty 50% nano-montmorillonite dispersion and 20% lime putty 80% nano-montmorillonite dispersion	Assessment of pozzolanic activity	Heating rate of 10°C/min under nitrogen flow up to 1000°C	@105–300°C: dehydration of lime putty and surfactant @400–550°C: dehydroxylation of $Ca(OH)_2$ and nano-montmorillonite @600–810°C: decomposition of $CaCO_3$ and nano-montmorillonite	Consumption of $Ca(OH)_2$ towards the production of additional C–S–H directly correlated with compressive strength increase	[33]
PC replacement at 1 wt% of organically modified montmorillonite @ different cation exchange degrees 0.6, 0.8, and 1.0 and at water-to-solid ratio of 0.27	Pozzolanic activity vs cation exchange degree	TGA @7, 28 and 56 days After predrying, the samples were heated up to 900°C at 10°C/min rate in a flowing nitrogen atmosphere	Mass loss up to 110°C: loss of adsorbed water and part of C–S–H @110–220°C: loss of interlayer water of C–S–H and dehydration of C-A-H, C-A-S-H and C-A-C-H, @400–475°C: dehydroxylation of $Ca(OH)_2$ @550–760°C: decomposition of complex mixture of carbonated phases, calcite and structural OH groups from hydrated calcium silicates	The content of hydration products was specified by simultaneous thermal analysis (STA)—differential scanning calorimetry (DSC) and thermogravimetry analysis (TGA). OMT with cation-exchange degree of 0.8 seems to be more suitable for cement substitution than OMT of higher cation exchange degree.	[34]
Synthetic C–S–H by hydration of C_3S in excess of water compared to C-S-H+ nS particles or C–S–H+ amine functionalized nS particles	Determination of amount of water and carbonation	Heating rate of 5°C/min under nitrogen flow up to 800°C	For the nS addition: 20–200°C corresponds to adsorbed and C–S–H water loss 200–800°C: silanol groups condense to siloxanes For the functionalized nS addition: 20–200°C corresponds to adsorbed and C–S–H water loss 200–400°C: silanol groups condense to siloxanes 450–800°C: decomposition of amino group (only for the functionalized nS mix)	The addition of nS particles inhibited the formation of carbonated phases, reducing C-S-H carbonations and increased the length of the silicate chains, reducing the size or the gel pores in C–S–H.	[35]
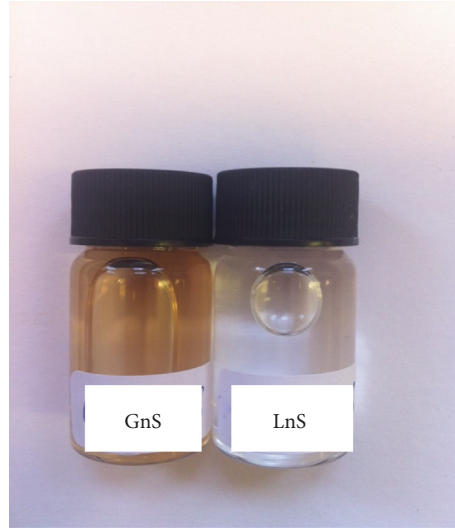
Figure 2: GnS carboxylic solution and LnS aqueous solution.

Table 2: Mix proportions (%) by total mass of solids.

	PC (%)	LS (%)	FA (%)	μS (%)	nS (% solids)	w/b
Mix						
PC43LS20FA43 (0% nS)	43	20	37	0.0	0.0	0.3
Quaternary mixes						
PC43LS19.9FA37 + 0.1% nS	43	19.9	37	0.0	0.1	0.3
PC43LS19.8FA37 + 0.2% nS	43	19.8	37	0.0	0.2	0.3
PC43LS19.5FA37 + 0.5% nS	43	19.5	37	0.0	0.5	0.3
PC43LS19FA37 + 1.0% nS	43	19	37	0.0	1.0	0.3
Quinary mixes						
PC43LS17FA37 + 2.5% μS + 0.5% nS	43	17	37	2.5	0.5	0.3
PC43LS17FA37 + 2.0% μS + 1.0% nS	43	14	37	2.0	1.0	0.3
PC43LS14FA37 + 5.5% μS + 0.5% nS	43	14	37	5.5	0.5	0.3
PC43LS14FA37 + 5.0% μS + 1.0% nS	43	17	37	5.0	1.0	0.3

matrix of the quaternary cement pastes was given by the following equation:

$$PC(43) + LS(20 - x) + FA(37) + nS(x), \quad (1)$$

where x = % of nS solids by mass, ranging from 0 to 1.0%.

These pastes were also mentioned to as PC/FA = 1.16 pastes.

2.2.2. Formulation of Quinary Cementitious Nanocomposite Binders.

Continuing the enhancement of reference paste PC43LS20FA37, four additional paste formulations were designed for each of the two nS types containing silica fume (μS) in addition. Again, the PC content was kept constant and the content of nS solids was deducted from the LS content for the reason mentioned above. The water-to-binder (w/b) ratio was kept at 0.3. The quinary pastes were prepared in the following proportions:

$$PC(43) + LS(20 - y - x) + FA(37) + \mu S(y) + nS(x), \quad (2)$$

where y = % of μS solids by mass, ranging from 2.0% to 5.5%, and x = % of nS solids by mass, ranging from 0 to 1.0%.

The mixing procedure, casting, demoulding, and curing are described elsewhere [7, 10]. In general, dry mixing of the powders took place first, with a spatula by hand. Then, water was stirred together with the nanoparticles, consecutively poured to the powders and mixed with an automatic dual shaft mixer at 1150 rpm for 3 minutes for pastes up to 300 g, time increasing with amounts of paste. The various formulations were air cured for 24 hours and then demoulded and water cured until the day of testing.

2.2.3. Material Preparation and Analytical Techniques

(1) Characterization of Nanosilica. Both nanosilica dispersions were characterized in terms of shape and size via transmission electron microscopy (TEM) and elemental composition via scanning electron microscopy/X-ray energy dispersive spectroscopy (SEM/EDX).

Transmission Electron Microscopy (TEM). Suspensions of 10 ng/ml were prepared from the LnS with distilled water. Small drops of the diluted solutions were then deposited on copper mesh grids coated with a thin carbon film. Grids were dried at 25°C prior to the

insertion in the instrument. Samples were examined at a voltage of 120 kV with a GATAN Jeol JEM 1200 mkII. Images were recorded on a Gatan Dual View camera.

Scanning Electron Microscopy/X-Ray Energy Dispersive Spectroscopy (SEM/EDX). For SEM/EDX elemental composition analyses, the LnS dispersion was first vacuum-dried for three days at a pressure of 10–2 mbar (100 Pa). The dried dispersion samples were placed uncoated on a sheet of molybdenum, an element absent from the LnS dispersions for unbiased elemental analyses. A matrix of 5×5 spectra was acquired, and the median of the elemental composition was presented. Samples were imaged using a Jeol 6480 LV SEM.

The exact same experimental procedure (TEM and SEM/EDX) was followed for the characterization of GnS. Images and analyses can be traced in the literature [10].

(2) Characterization of Pastes. For the characterization of the pastes, arrest of hydration was performed following two different methodologies: solvent exchange and oven drying as described by Calabria-Holley et al. [36]. For SEM backscattered (BSC) image generation and microstructural investigation, solvent exchange was preferred for the arrest of hydration. Isopropanol was selected as the most appropriate solvent according to the literature [37, 38]. The thermal properties were investigated via thermal gravimetric analysis and differential thermogravimetry (TGA/dTG). For TGA/dTG, the oven drying technique was adopted.

Compressive Strength. All mixes were tested at a loading speed of 0.5 MPa/s. The mean compressive strength was obtained by testing three to six cylindrical specimens per mix. Therefore, the compressive strength results presented herein refer to the mean measured.

Thermal Gravimetric Analyses (TGAs). Thermal gravimetric analyses were carried out using a Setaram TGA92 instrument. Twenty milligrams of each mix was placed in an alumina crucible and heated at a rate of 10°C/min from 20°C to 1000°C under 100 mL/min flow of inert nitrogen gas. The differential thermal gravimetric (DTG) curve was derived from the TG curve. Buoyancy effects were taken into account, by correcting the curves via automatic blank curve subtraction.

Three different areas are compared, depending on the hydration products thermally decomposing between specific temperature ranges, as measured by the thermogravimetric (TG) analyses [9, 10]:

The first one is related to the dehydration of C–S–H, ettringite, gehlenite, and monosulfate, between 100°C and 200°C. It can be postulated that the greater the loss measured, the greater the amount of C–S–H and ettringite produced by the hydration of the paste.

The second area of interest is associated with the dehydration of $Ca(OH)_2$ between 440°C and 510°C.

The third area of interest is the decomposition of $CaCO_3$ occurring between 700°C and 810°C.

Microstructural Characterization by Scanning Electron Microscopy (SEM). A set of SEM images was collected for each formulation at different ages (1 day, 28 days, and 56 days). A backscattered electron (BSE) detector was used to capture images of the as received, uncoated samples.

(3) Mathematical Elaboration. Correlating hydration characteristics with mechanical strength performance in cementitious nanocomposite binders.

The high correlation between the consumption of calcium hydroxide towards the formation of hydration products (microscale characteristics) and the delivered compressive strengths (macroscale performance) of the nS-modified pastes with respect to time has been expressed through a newly introduced ratio. This ratio comprises of the compressive strength of the pastes versus the $Ca(OH)_2$ content, as detected by the TGA/dTG analyses, plotted against time. It was found to give an interesting representation of the performance of cement nanocomposites [9, 10].

3. Results and Discussion

3.1. Characterization of Nanosilica. TEM analysis showed that the diameter of the LnS particles ranged from 8 nm to 50 nm (Figure 3(a)) and that they were homogenously dispersed and highly concentrated layers of nS on top of other layers of nS (Figure 3(b)). The diameter of the GnS particles was about 5–8 nm, and images can be found in the literature [10].

A 5×5 matrix of spectra was collected for GnS and LnS in each elemental analysis (SEM/EDX). In Figure 4, the comparison of the elemental compositions of the two different nS dispersions shows that GnS exhibits traces of SiO_2 and over 70% (normalized atomic) carbon content, confirming the presence of polycarboxylates. It should be noted that, in GnS, the hydrocarbon present is more prone than the nS itself to have significant effects in the cement pastes. LnS, however, comprises of almost pure SiO_2 and therefore expected to perform as a pure, aqueous nS dispersion, exploiting the benefits of nanoparticles discussed before such as the high surface area or due to the high SiO_2 increase in the C–S–H, when added to cement paste formulations.

3.2. Compressive Strength

3.2.1. Quaternary Cementitious Nanocomposite Pastes. Research on ternary nanocomposite binders comprising of Portland cement, limestone, and nano-SiO_2 has shown immediate reactivity of the nanoparticles with a simultaneous effect in strength gain, at day 1 [8, 9]. The strength development of the LnS quaternary cementitious nanocomposite binders is presented in Figure 5(a).

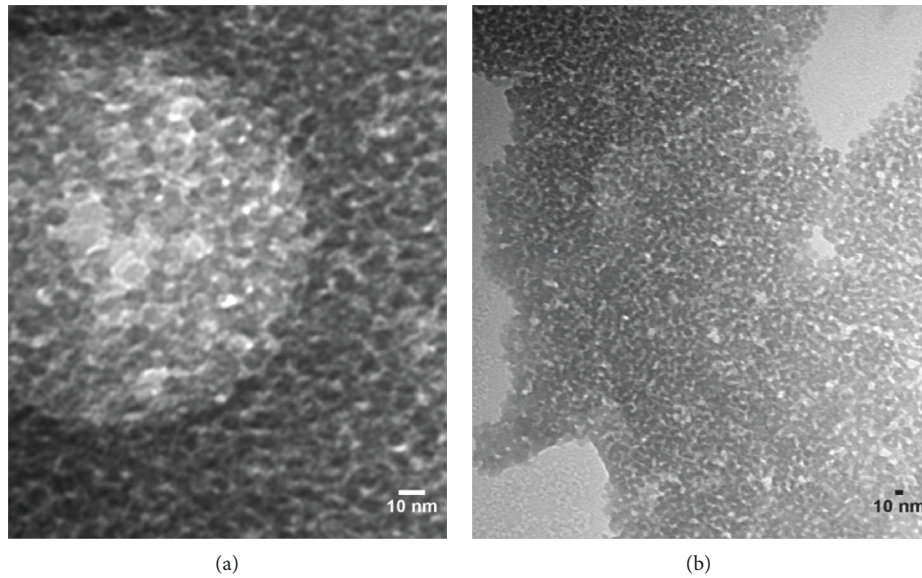It can be seen that LnS did not offer early strength gain (day 1). Adding to that, the reference paste reached a

(a)

(b)

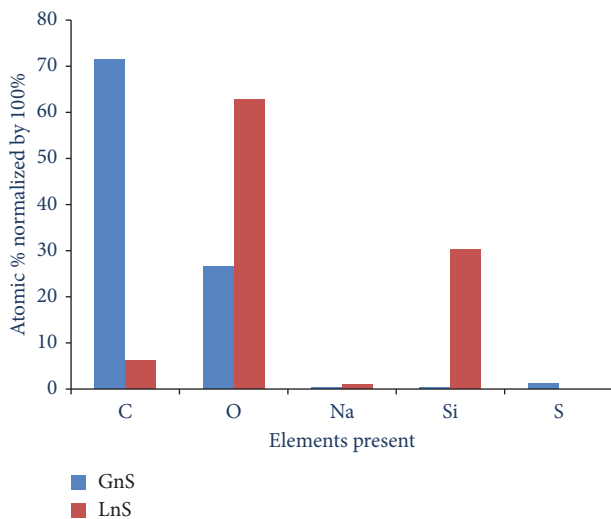Figure 3: TEM micrograph of LnS at (a) 500,000x and (b) 15,0000x magnification.

Figure 4: Comparison of the elemental composition of GnS and LnS.

observed for the LnS additions; all four formulations compared to the reference binder exhibit:

(i) Lower 1-day strength

(ii) Marginal strength gain between day 1 and 28, still lower than that of the reference binder

(iii) Gradual increase between day 28 and 56, but lower than that of the reference binder

(iv) Drastic increase between day 56 and 90, with 0.5% LnS surpassing the strength of the reference binder

As discussed by Calabria-Holley et al. [39], Papatzani et al. [7], and Kawashima et al. [16], it is possible that, at higher nS concentrations, the hydration products formed by the immediate reactivity of the nS have higher C/S ratio in the C–S–H, creating dense wrapping around the FA particles, which are found in abundance in the paste. The C–S–H formed in presence of FA has a lower C/S ratio [40]; therefore, these "pockets" of dense C–S–H and ettringite may perform as ion penetration barriers, delaying even further the reaction of a part of the FA. It is the authors' opinion that, in low PC/FA ratio composite cement pastes, the presence of high contents of nS managed to "deactivate" part of the FA. In support to this argument, a number of unreacted FA particles surrounded be the "pockets" were identified by the SEM analyses and are presented in Section 3.6. This could be the reason why the specific binders delivered reduced compressive strength. For the lower LnS content pastes, their compressive strength is expected to increase further with age, mainly because with the advancement of time the contribution of FA to strength gain, and densification of the LnS-modified pastes will be more prominent.

With respect to the GnS addition, the long-term performance seems to be enhanced by the 0.5% by mass GnS addition. The presence of significant quantities

compressive strength of approximately 40 MPa at day 28, which was stagnant thereafter. This could be attributed to delayed PC and FA hydration, a hypothesis revisited and elaborated upon after the thermal analyses. Furthermore, neither did the two lower LnS contents (0.1 and 0.2% by mass) offer improvements in the compressive strength. The highest LnS (1%) leads to strength reduction at later ages, possibly attributed to the agglomeration of particles and/or some other mechanism discussed in detail below. To assess this hypothesis, SEM imaging was carried out at the 0.5% and the 1% nS binders, as well, as shown in Section 3.6.

In terms of determining the optimum amount of LnS particles for cementitious nanocomposite binders with PC/FA ratio of 1.16, the 0.5% by mass addition seemed to have the most favourable effect. Moreover, there is a pattern
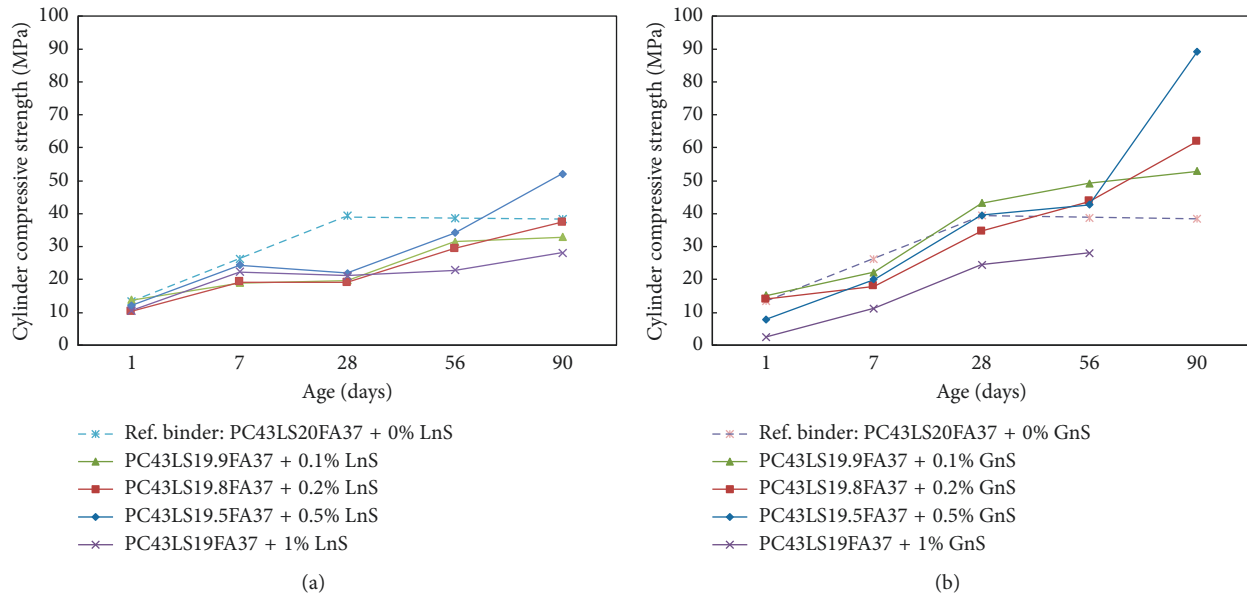
FIGURE 5: Cylinder compressive strength of (a) LnS and (b) GnS nanocomposite binders based on PC43LS20FA37.

of carbon seemed to have played a role in the performance of the GnS-modified pastes, as analyzed in the following sections. It should be mentioned that, during the production of the specimens, the ones with the higher w/b ratio exhibited prolonged setting, possibly because the polycarboxylates traced in the solution act as water reducing agents and therefore lower water quantities could have been added [10]. This, however, would have rendered the formulations incomparable amongst them and was, therefore, avoided.

The highest GnS addition (1% by mass) was proven the least favourable and the lowest (0.1% by mass) was beneficial for the early age compressive strength (Figure 5(b)). Overall, however, the 0.5% addition although at the early ages performed similar to the reference binder, at later ages it outperformed it.

After testing, the samples were examined for bad compaction and visual porosity. It can be observed that all LnS and GnS enhanced binders were well compacted for the lower nS addition and presented limited visual pores compared to those of the reference paste (Figure 6).

Further Comparisons. The following two graphs serve as a summary and comparison of the mechanical performance of the 0.1% and 0.5% nS modifications of PC43FA20LS37 at different ages (Figure 7). The stagnant compressive strength of the reference paste after day 28 was surpassed by both GnS additions, the 0.5% addition being the most advantageous. The 0.1% LnS addition delayed the strength gain, which was eventually enhanced only at the 0.5% LnS addition.

3.2.2. Quinary Cementitious Nanocomposite Pastes. The compressive strength of two sets of quinary binders are presented, both based on PC43LS20FA37. The first was

modified by the addition of μS and LnS and the second of μS and GnS. The addition of micro- and nanosized silica has been reported to reduce porosity and improve mechanical properties of cementitious nanocomposites, although the possibility of use of superplasticizers has also been acknowledged [41]. In this series, GnS is acknowledged to perform as a superplasticizer on its own [10]. The results are presented in Figure 7.

Once again, the specimens containing 0.5% nS by mass performed better than those containing 1% nS by mass. As shown in Figure 8, LnS exhibited greater potentials with the higher content of μS (5% by mass). However, the strength gain was delayed until day 90.

For the GnS-modified pastes, the specimens containing 0.5% GnS by mass performed better than those containing 1% GnS by mass. As shown in Figure 8(b), GnS performed better in combination with the lower μS content (2.5% by mass). However, even in the case of GnS, strength gain was only achieved after day 56. The FA, μS, and nS particles in these quinary formulations compete for the consumption of the $Ca(OH)_2$ produced by cement hydration. Hence, the pozzolanic reactions must have been delayed.

After testing, the samples were examined for bad compaction and visual porosity. It can be observed that all LnS- and GnS-enhanced binders were well compacted for the lower μS + nS addition and presented limited visual pores compared to those of the reference paste (Figure 9).

3.3. Thermal Gravimetric Analyses

3.3.1. Quaternary Cementitious Nanocomposite Pastes. The results of the TG analyses on the four different combinations of LnS on PC43LS20FA37 are shown in

Cylinders crushed by compression at 90 days-
Quaternary binders

(i) Visual porosity

(ii) Compaction issues

(iii) Fracture mode: typical for reference paste and brittle for
nanocomposite binders

PC43LS20FA37

PC43LS19.9FA37 + 0.1% LnS   PC43LS19.8FA37 + 0.2% LnS   PC43LS19.5FA37 + 0.5% LnS   PC43LS19FA37 + 1.0% LnS   LnS

PC43LS19.9FA37 + 0.1% GnS   PC43LS19.8FA37 + 0.2% GnS   PC43LS19.5FA37 + 0.5% GnS   GnS

FIGURE 6: Crushed cylinders of LnS or GnS nanocomposite binders based on PC43LS20FA37.

(a)

(b)
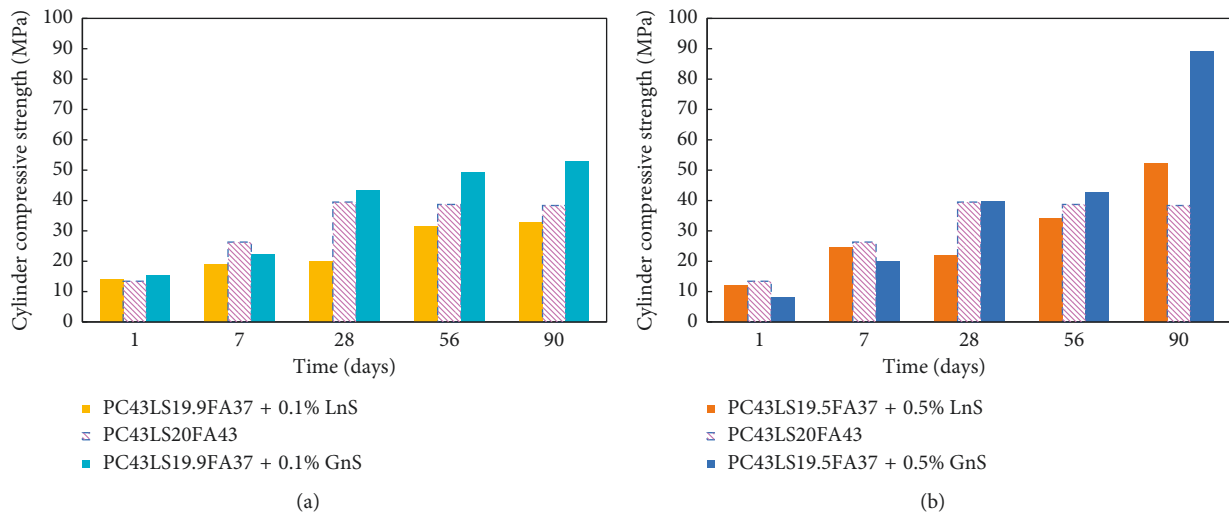
FIGURE 7: Comparison of the (a) 0.1% GnS or 0.1% LnS and (b) 0.5% GnS or 0.5% LnS modification of cementitious nanocomposite binders based on PC43LS20FA37.

Figure 10. The drastic reduction in the $Ca(OH)_2$ content observed at day 56 in Figure 10 could be related to the marginal increase in $CaCO_3$ observed at the same age, implying the occurrence of carbonation rather than chemical reactivity of the LS present in the paste. On the contrary, the TGA curves, covering 0–1000°C, presented in

Figure 11 showed a significant increase in the C–S–H and ettringite directly linked with the consumption of $Ca(OH)_2$ content from day 28 to day 56 and, consequently, the strength gain observed at these ages for specific pastes. Additionally, the following can be observed in the graphs that follow:
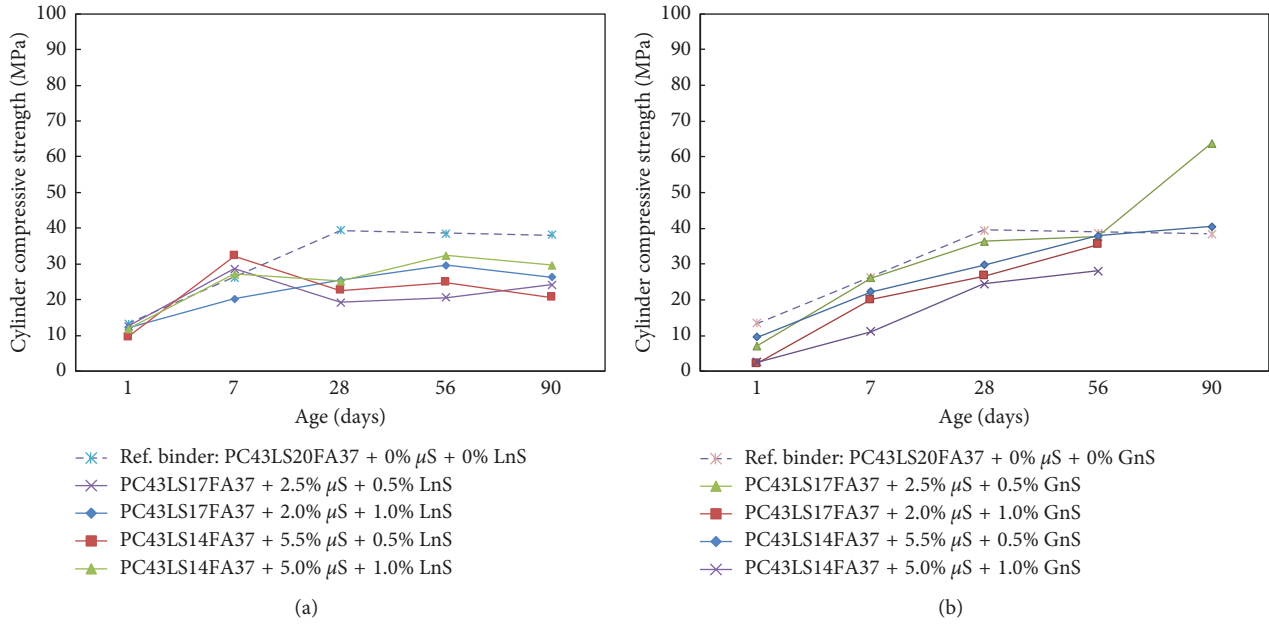
FIGURE 8: Cylinder compressive strength of μS and (a) LnS or (b) GnS nanocomposite binders based on PC43LS20FA37.
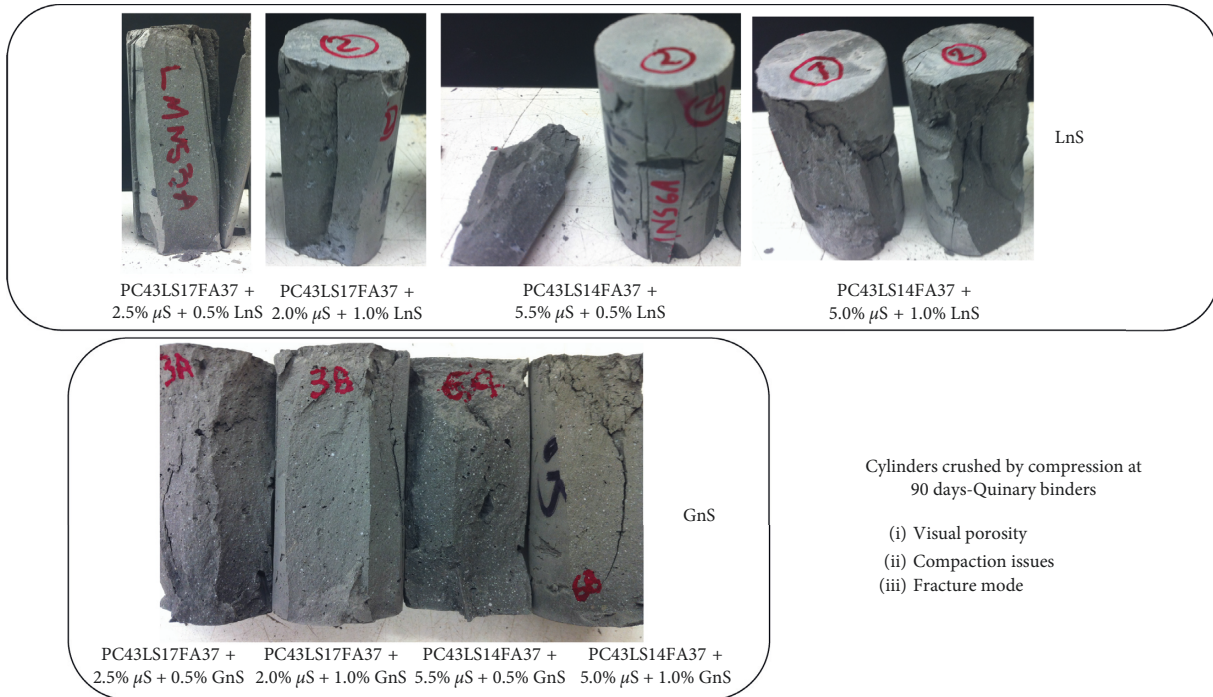

FIGURE 9: Crushed cylinders of μS and LnS or μS and GnS nanocomposite binders based on PC43LS20FA37.

(i) Significant increase in the $Ca(OH)_2$ content from day 1 until day 7 in agreement with the results on PC65LS05FA30 presented by De Weerdt et al. [42]

(ii) From day 7 to 28, there were subtle changes in the $Ca(OH)_2$ content

It is approximated that, when PC hydrates produces about 20–25% by mass $Ca(OH)_2$ at day 28 [43]. Also, in the same research, the degree of FA reaction has been identified as approximately 13% of the total FA content at day 28, reaching about 25% at day 90; therefore, of the 37% FA, 4.81% is expected to have reacted at day 28.

Moreover, at day 28, 43% by mass PC alone should have produced approximately 10.75% ($43 \times 25\%$) $Ca(OH)_2$. The TG analyses, at day 28, detected 6% $Ca(OH)_2$; therefore, a very small amount of the reactive by day 28 FA (summing up to 1/4 of the total FA content) was left to react after day 28. Theoretically, at day 56, the $Ca(OH)_2$ content detected in the
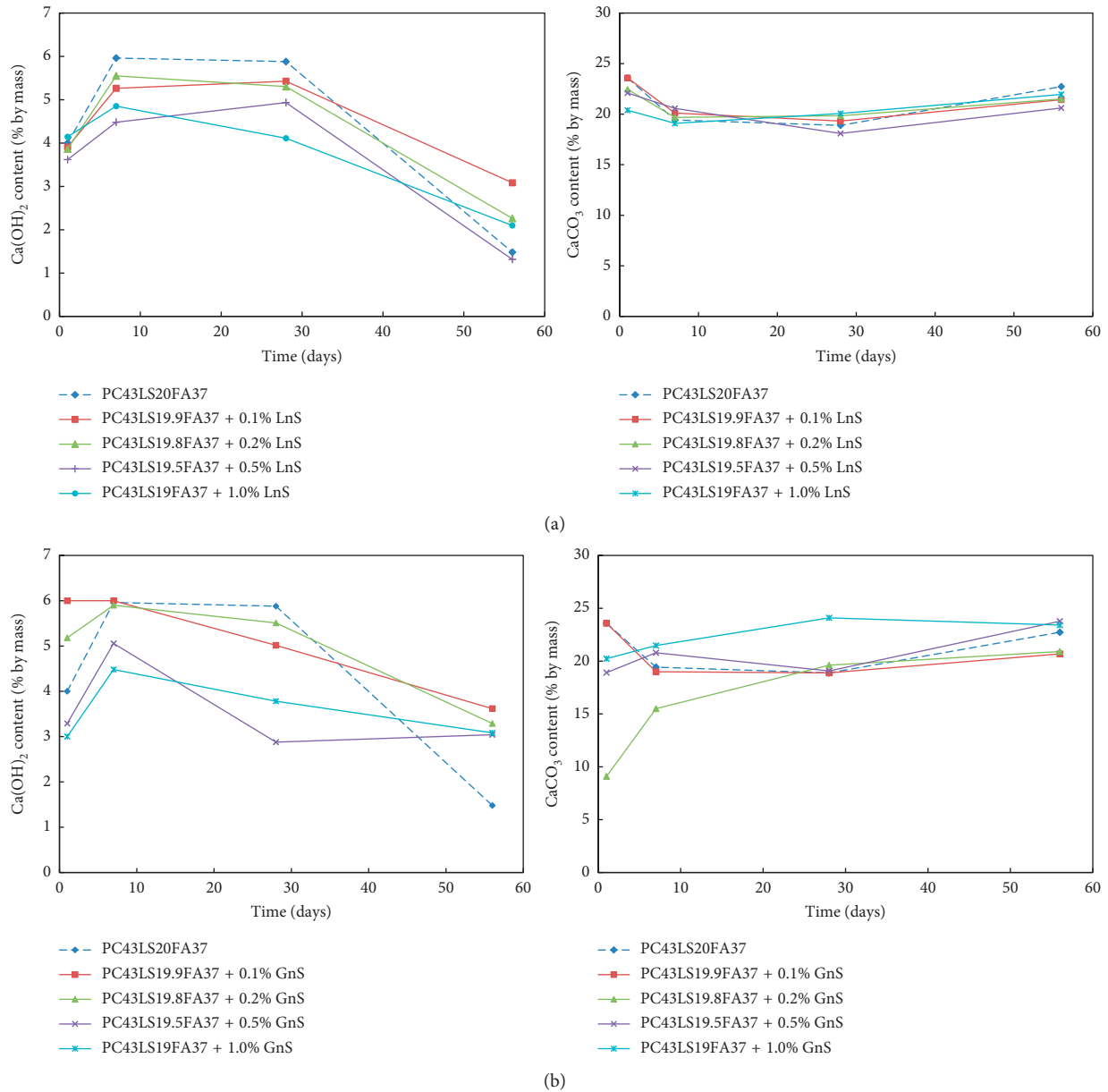
(a)

(b)

FIGURE 10: $Ca(OH)_2$ and $CaCO_3$ content of (a) LnS and (b) GnS nanocomposite binders based on PC43LS20FA37.

reference paste was expected to be lower than that of day 28. If it is assumed that another 5.5% of FA has reacted by day 56, then the $Ca(OH)_2$ content detected in the reference paste PC43LS20FA37 should have been equal to $6-5.5 = 0.5\%$. The TG analyses showed that there was 1.5% of $Ca(OH)_2$, indicating further hydration of PC and possible delayed reactivity of the FA, certainly, though, there was no indication of depletion of $Ca(OH)_2$ by the FA. Lastly, it should be acknowledged that some carbonation of the reference paste may have taken place, since a mass loss was detected after 860°C in Figure 11. However, the same evidence was present for almost all pastes at day 28 as displayed in Figure 11; therefore, relative comparisons are valid.

It is the author's opinion that the evolution of strength gain for these series of pastes could be described in the following chronological scenario.

By day 1, the hydration of PC had started and the LnS particles, being highly reactive, as shown in the less complex pastes in literature [7, 8], were immediately engaged in reactions consuming $Ca(OH)_2$ formed by the hydration of cement. The C–S–H produced by LnS reactivity has a lower C/S ratio and a denser nature than the reference paste [39].

Between day 1 and day 7, PC had further hydrated; the remaining LnS particles were completing their participation expanding the C–S–H network around particles of PC, LS, and FA. Moreover, a part of the FA particles had started feeding from the $Ca(OH)_2$ formed by PC hydration. Another part was yet to react, but remained covered by the dense C–S–H formed by LnS. Additionally, the abrupt lowering of the pH by the catalytic reactions of LnS may not have allowed the vitreous phase of a part of the FA particles
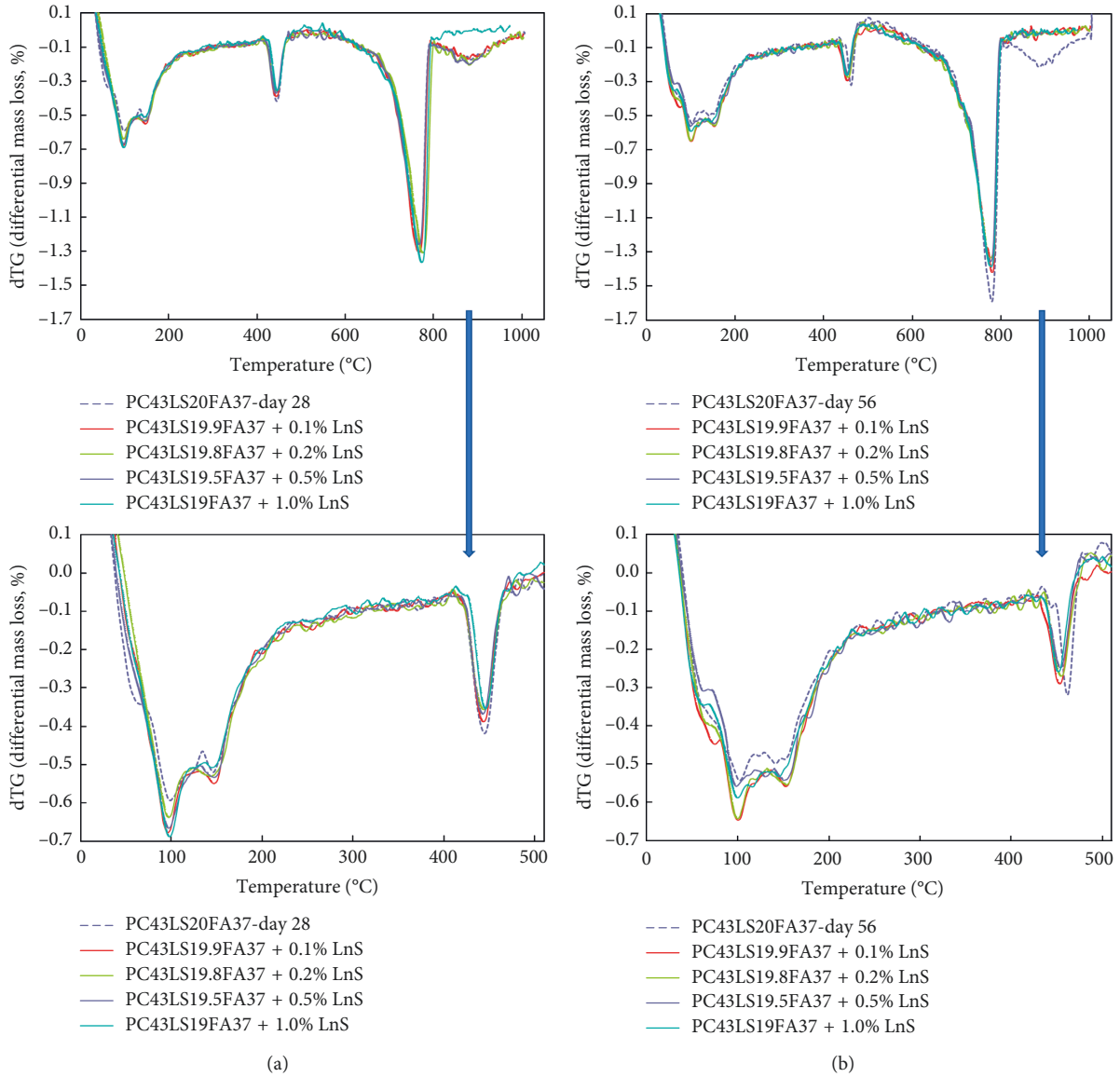
FIGURE 11: Differential mass loss of LnS nanocomposite binders based on PC43LS20FA37 (a) at day 28 and (b) at day 56.

to decompose and subsequently engage in additional pozzolanic reactions [10].

At day 7, the TG analyses inferred that, in such pastes with high FA content, the pozzolanic reactions were the primary consumers of $Ca(OH)_2$, particularly since most of the LnS had already reacted in the lower LnS content nanocomposite binders.

By day 28, the lower LnS content nanocomposite binders did not consume any more $Ca(OH)_2$, but neither did the FA particles due to the ion barriers set by the LnS hydration products.

However, as age advanced, possibly lowering the pH of the hydrating paste, the FA attraction of $Ca(OH)_2$, exceeded the strength of the bonds surrounding the FA particles another part of which started to react, consuming the available $Ca(OH)_2$.

By day 56, further strength gain was achieved by the LnS contents up to 0.5% by mass and significant amounts of

$Ca(OH)_2$ were still noticeable. Therefore, the theory presented by other researches on the depletion of $Ca(OH)_2$ in such pastes was not confirmed in this research. For example, Kawashima et al. [16] who studied ternary nanomodified Portland cement binders of high PC/FA ratio equal to 1.5 found that water cured at $60^{\circ}C$ samples showed signs of $Ca(OH)_2$ depletion at day 7.

In contrast to this, the chronological scenario is shedding more light in the complex processes taking place in cementitious nanocomposite binders and is by no means dogmatic. Evidences rendered the theory of competition between FA and nS particles in such binders more adequate to explain the complex phenomena [10, 31, 39, 44].

The suggestions should be investigated by the nanoindentation method, which can provide information on the C/S ratio and stiffness moduli [45]. Furthermore, a series of X-ray tomography (CT) scans could also
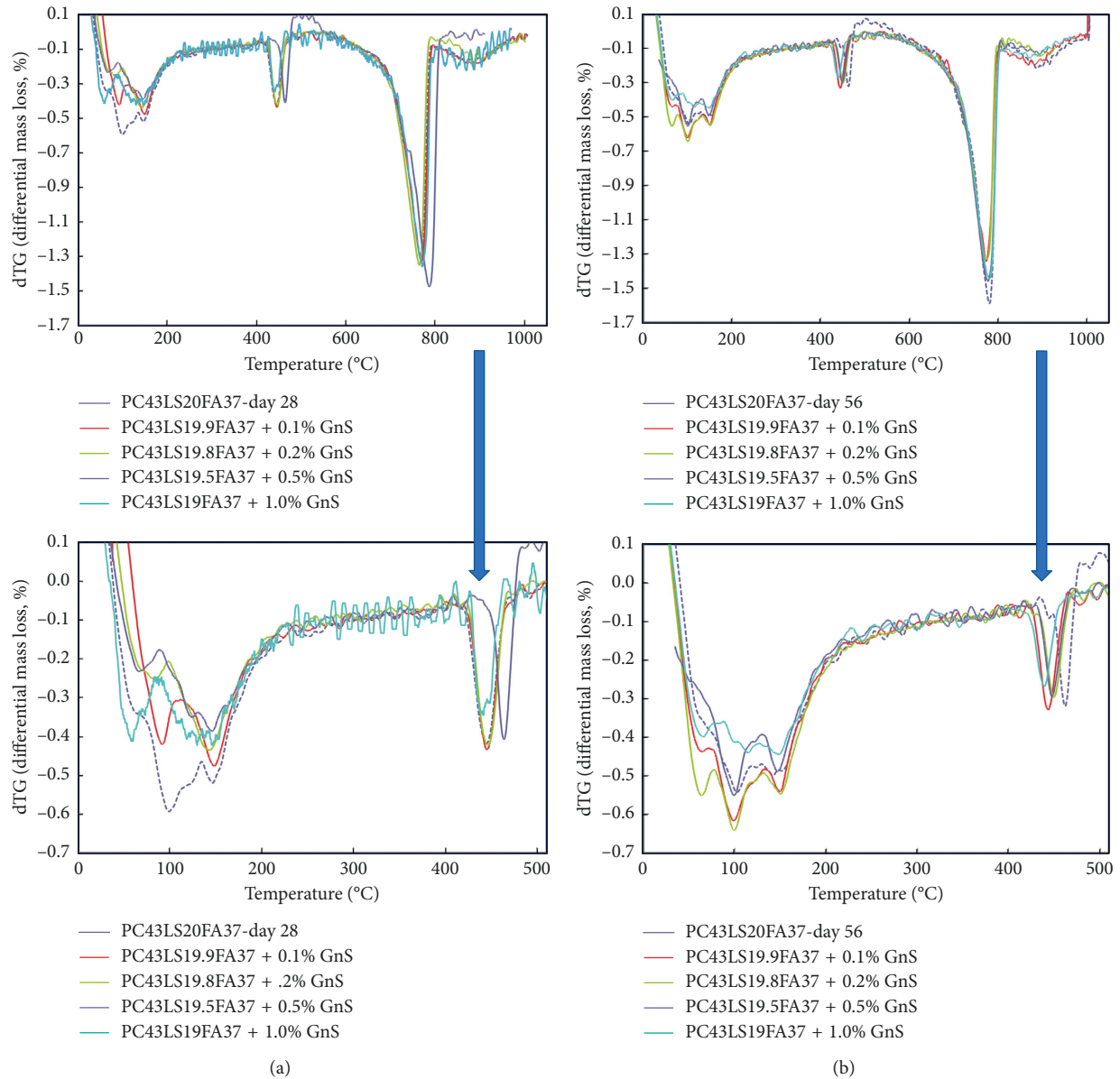
Figure 12: Differential mass loss of GnS nanocomposite binders based on PC43LS20FA37 at (a) day 28 and (b) day 56.

bridge the relationship between densification of C–S–H in the presence of lower LnS contents and probable increase in porosity due to the presence of excessive LnS particles.

A short reference to the ettringite formation should also be made. Knowing that the specific FA used contained impurities and sulfates, it was no surprise that greater quantities of ettringite were formed [46], as can be observed in Figure 11.

As shown in Figure 12, the addition of GnS affected the consumption of the $Ca(OH)_2$ content at day 1 and 7, for the two higher GnS concentrations, whereas its effect was more evident after day 28. The 1% GnS dosage seemed to be creating more carbonate formations with the mass loss in the decarboxylation temperature range between 650 and 800°C, showing an increase with respect to the other specimens.

However, as discussed earlier, the presence of high contents of polycarboxylates in the dispersion could be responsible for this response.

3.3.2. Quinary Cementitious Nanocomposite Pastes. It is interesting to note the similarities between the graph depicting the $Ca(OH)_2$ consumption in the LnS-modified pastes (Figure 10) and the one for the μS- and LnS-modified pastes (Figure 13). The only difference between the two is the slightly greater consumption of the latter, attributed to μS. Once again, the 0.5% LnS combination showed better performance by consuming more $Ca(OH)_2$ at later ages. The samples did not show signs of carbonation (Figure 13). In fact, for the first two samples at the lower μS content, the LS content was reduced to 17% by mass, and the $CaCO_3$ detected was of this order. The same was valid for the other
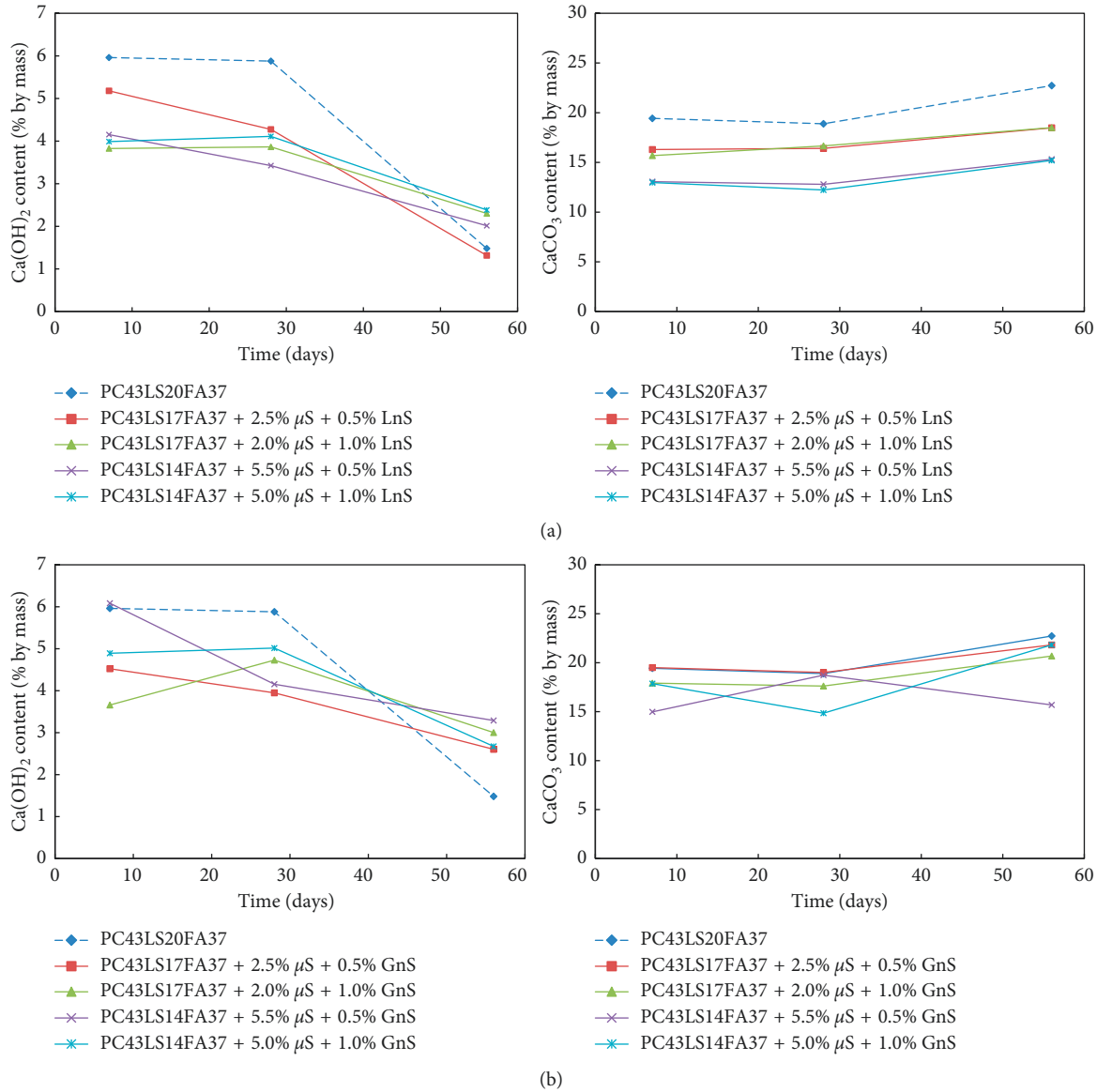
(a)

(b)

FIGURE 13: Ca(OH)$_2$ and CaCO$_3$ content of μS and (a) LnS or (b) GnS nanocomposite binders based on PC43LS20FA37.

two samples at the higher μS content, in which LS was reduced to 14% by mass. Furthermore, the differences in the TG analyses of the 28-day old and 56-day old μS/nS binders can be observed in Figure 14. The consumption of Ca(OH)$_2$ is evident with simultaneous production of additional C–S–H.

The trend in Ca(OH)$_2$ consumption in the μS- and GnS-modified pastes is almost identical to the one delivered by the GnS-modified quaternary binders (Figure 15). The overall consumption is slightly lower, though, due to the reactivity of μS. Two things should be noted: (i) the 0.5% GnS with 2.5% μS binder consumed greater quantities of Ca(OH)$_2$ and (ii) it was this paste that exhibited the best compressive strength performance. Furthermore, there were no indications of carbonation having taken place.

3.4. *Crystallographic Analyses of Quaternary Cementitious Nanocomposite Binders.* The X-ray diffraction analyses shown in Figure 16 confirmed all the above findings:

(i) Production of additional ettringite from day 1

(ii) Production of additional C–S–H from day 1

(iii) Increase of Ca(OH)$_2$ content at day 1 with subsequent reduction at later ages, leading to elimination of the detectable (non-encapsulated by C-S-H) Ca(OH)$_2$ by day 56

(iv) Absence of carboaluminate hydrates (expected to give diffractions at 10.8° 2θ, for hemicarbonate, and 11.7° 2θ for calcium monocarbonate hydrate [42], even by day 56, a finding which was not totally clear by the TG analyses).
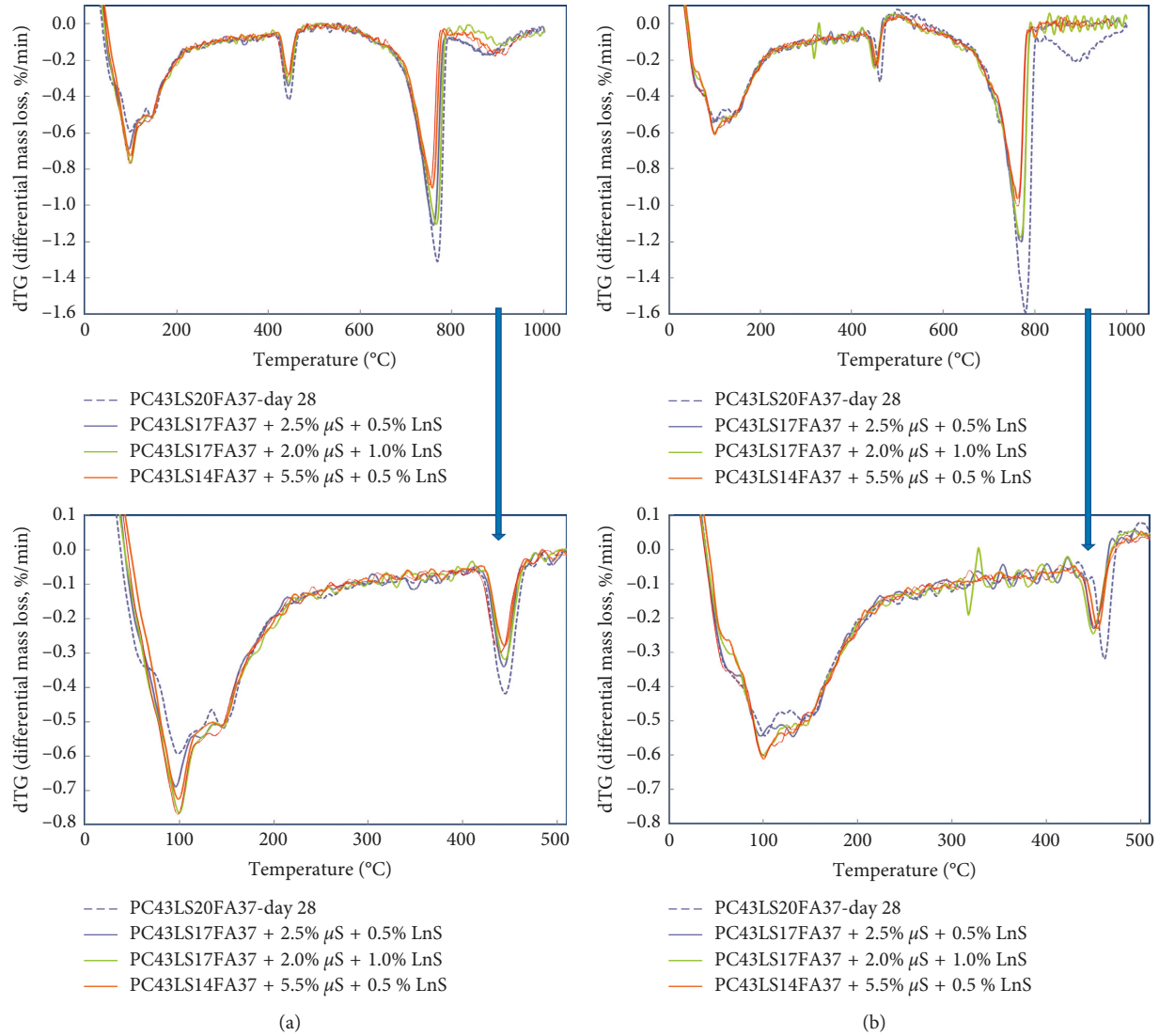
FIGURE 14: Differential mass loss of LnS and μS nanocomposite binders based on PC43LS20FA37 between 0 and 1000°C at (a) day 28 and (b) day 56.

3.5. Correlation of Microscopic with Macroscale Results

3.5.1. Quaternary Cementitious Nanocomposite Binders. Lastly, the theory presented elsewhere [10] on the correlation of microscopic results of $Ca(OH)_2$ content with macroscale results of compressive strength tests was verified in the LnS-modified series, as well as shown in Figure 17(a), confirming at one glance that the 0.5% LnS modification was the most effective of all, overall, exhibiting the greatest $Ca(OH)_2$ consumption. Moreover, this relationship was verified in the GnS-modified series on PC43LS20FA37, as shown in Figure 17(b), confirming at one glance that the 0.5% GnS modification was the most effective of all, overall.

3.5.2. Quinary Cementitious Nanocomposite Binders. Lastly, the abovementioned relationship was further tested in the μS- and GnS-modified quinary series, as well as shown

in Figure 18, confirming at one glance that it is the GnS content the primary factor influencing the performance rather than the μS contents. Moreover, the 0.5% GnS modification offered more effective pastes.

3.6. Microstructural Investigation of PC/FA = 1.16 LnS-Modified Quaternary Cementitious Nanocomposite Binders. Backscattered (BSC) SEM micrographs of day 1, day 28, and day 56 are presented. With respect to the reference paste, PC43LS20FA37, the following can be observed in Figure 19:

  (i) Densification of the paste has taken place by day 28 accompanied by reduction in microcracks. In other words, capillary porosity and microcracks reduce with nS content and age advancement.

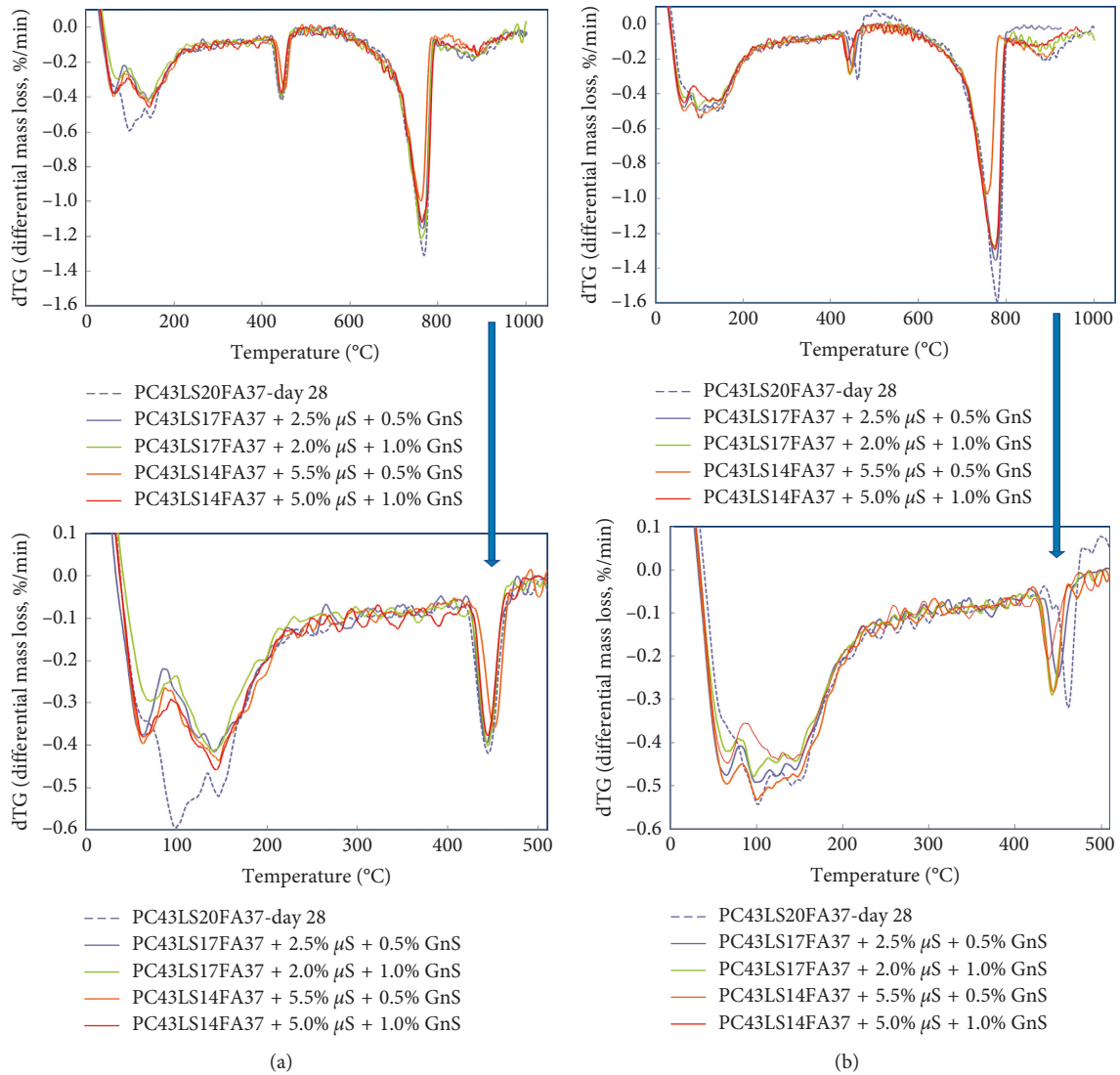 (ii) A number of unreacted FA (denoted by uFA) particles, surrounded by "pockets" as discussed in

FIGURE 15: Differential mass loss of GnS and μS nanocomposite binders based on PC43LS20FA37 between 0 and 1000°C at (a) day 28 and (b) day 56.
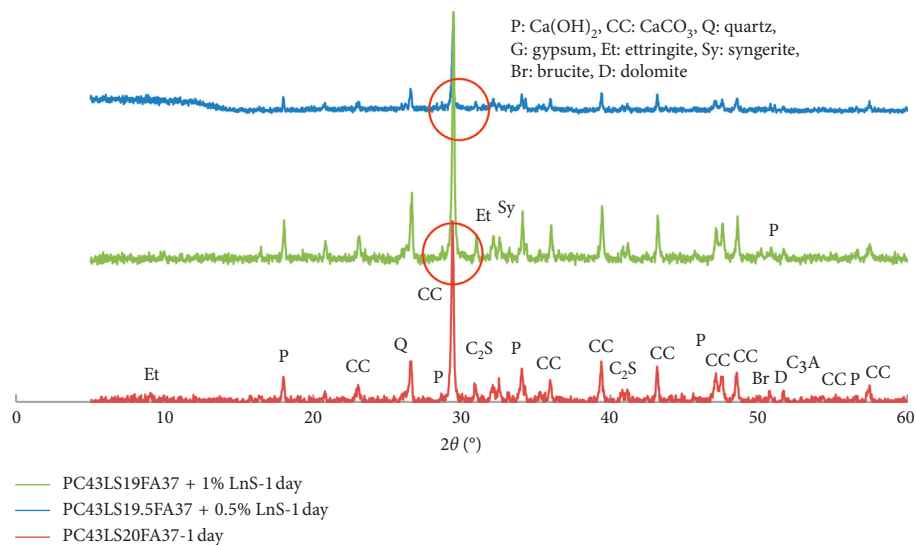

(a)

FIGURE 16: Continued.

P: Ca(OH)$_2$, CC: CaCO$_3$, Q: quartz,
G: gypsum, Et: ettringite, Sy: syngerite,
Br: brucite, D: dolomite

2θ (°)

——— PC43LS19FA37 + 1% LnS-7 days
——— PC43LS19.5FA37 + 0.5% LnS-7 days
——— PC43LS20FA37-7 days

(b)

P: Ca(OH)$_2$, CC: CaCO$_3$, Q: Quartz,

2θ (°)

——— PC43LS19FA37 + 1% LnS-28 days
——— PC43LS19.5FA37 + 0.5% LnS-28 days
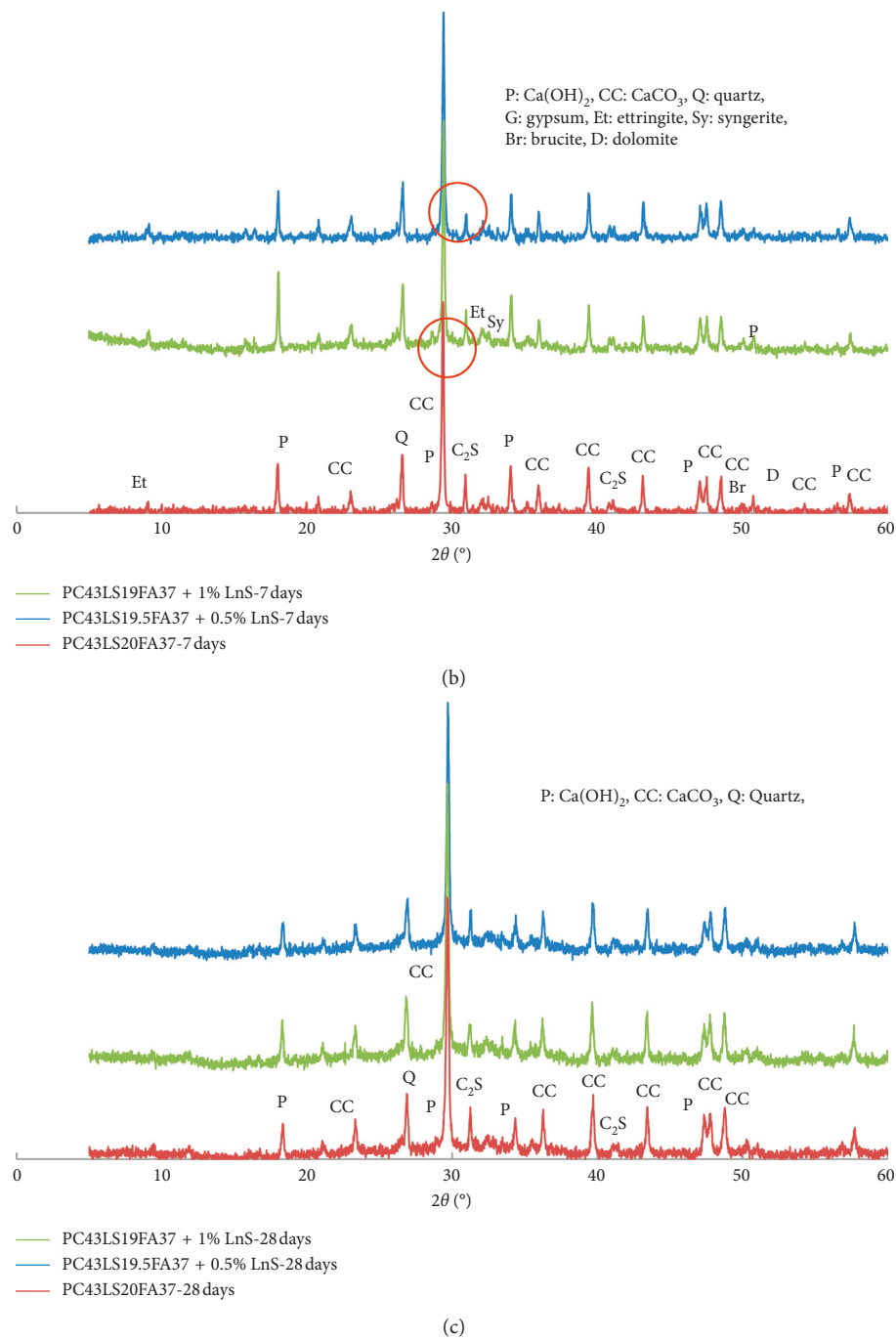——— PC43LS20FA37-28 days

(c)
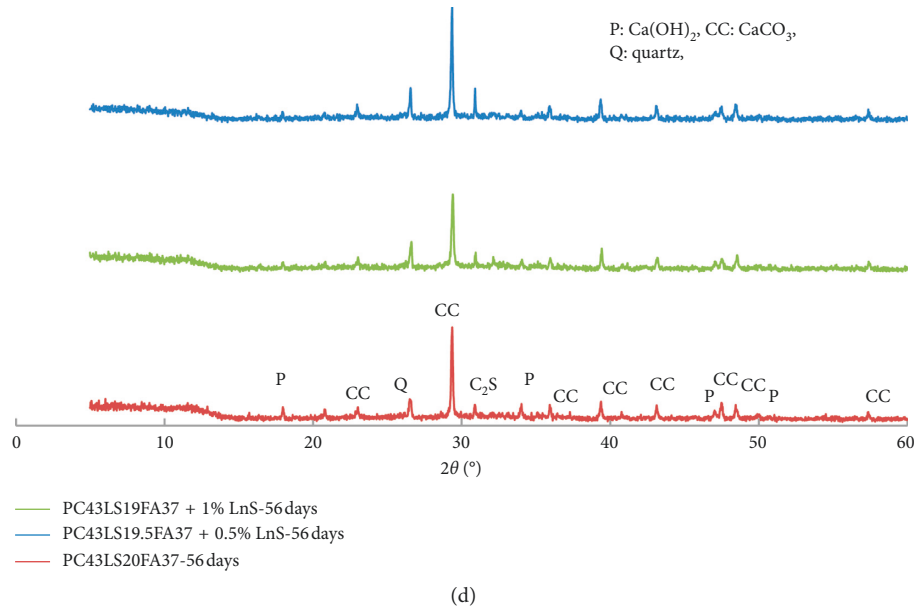
FIGURE 16: Continued.

(d)

FIGURE 16: XRD pattern of LnS nanocomposite binders based on PC43LS20FA37 at (a) day 1, (b) day 7, (c) day 28, and (d) day 56.
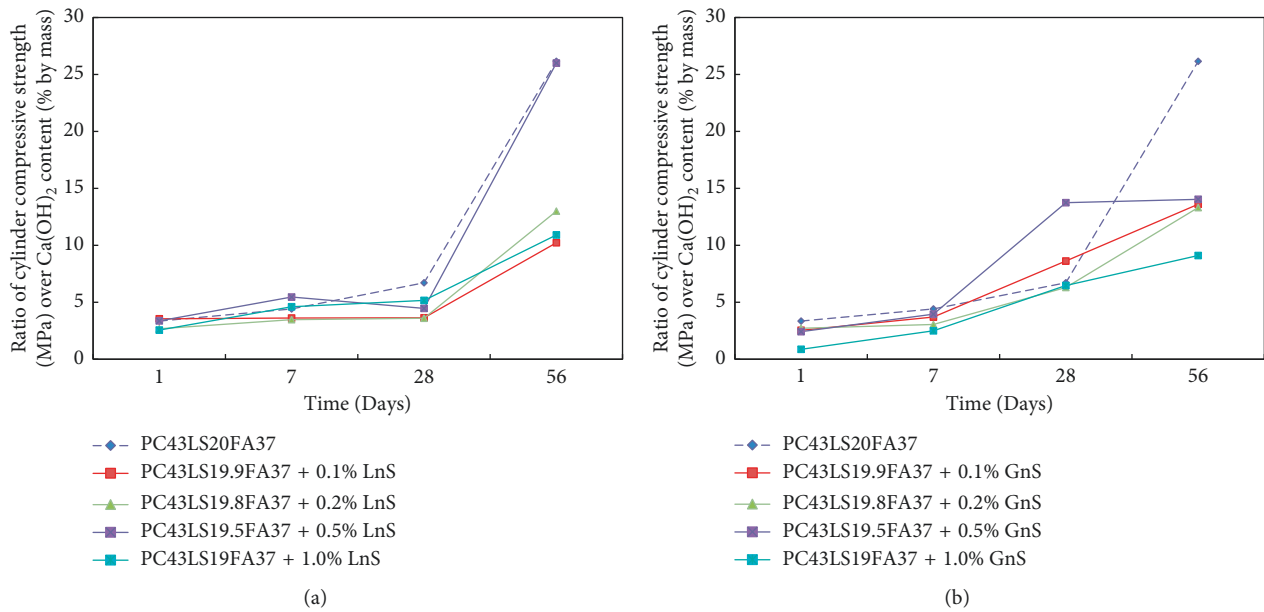

(a)

(b)

FIGURE 17: Relating microscale characteristics to macroscale performance of (a) LnS- and (b) GnS-modified nanocomposite binders based on PC43LS20FA37.

the previous sections, identified by their light colour and spherical shape are still visible by day 56, enforcing previous arguments.

(iii) Reacted FA (denoted by rFA) particles created seeding effect, by attracting needle-like hydration products reinforcing the hypothesis of greater FA activation by day 56.

(iv) Dense areas of what seems to be C–S–H (denoted by CSH on the micrographs) were distinguished. The dark rim around the formation was clearly visible.

(v) $Ca(OH)_2$ crystals (denoted by P) participating in the seeding effects in agreement with other studies [46].

Furthermore, the optimal LnS-modified paste, PC43LS19.5FA37 + 0.5% LnS, and the less favourable one, PC43LS19FA37 + 1% LnS, were also examined at the three different ages. With respect to PC43LS19.5FA37 + 0.5% LnS, the following can be noted:

(i) A highly-densified morphology by day 56 can be observed, possibly denser than that of the reference paste. The presence of microcracks seemed eliminated.
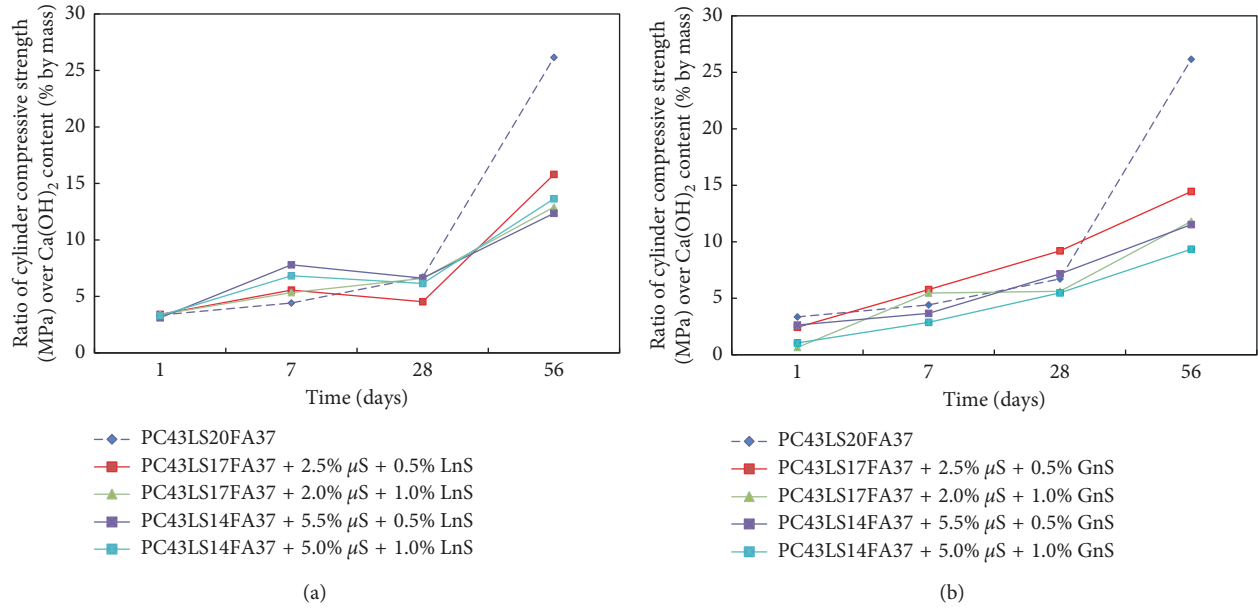
FIGURE 18: Relating microscale characteristics to macroscale performance of μS and (a) LnS- or (b) GnS-modified nanocomposite binders based on PC43LS20FA37.
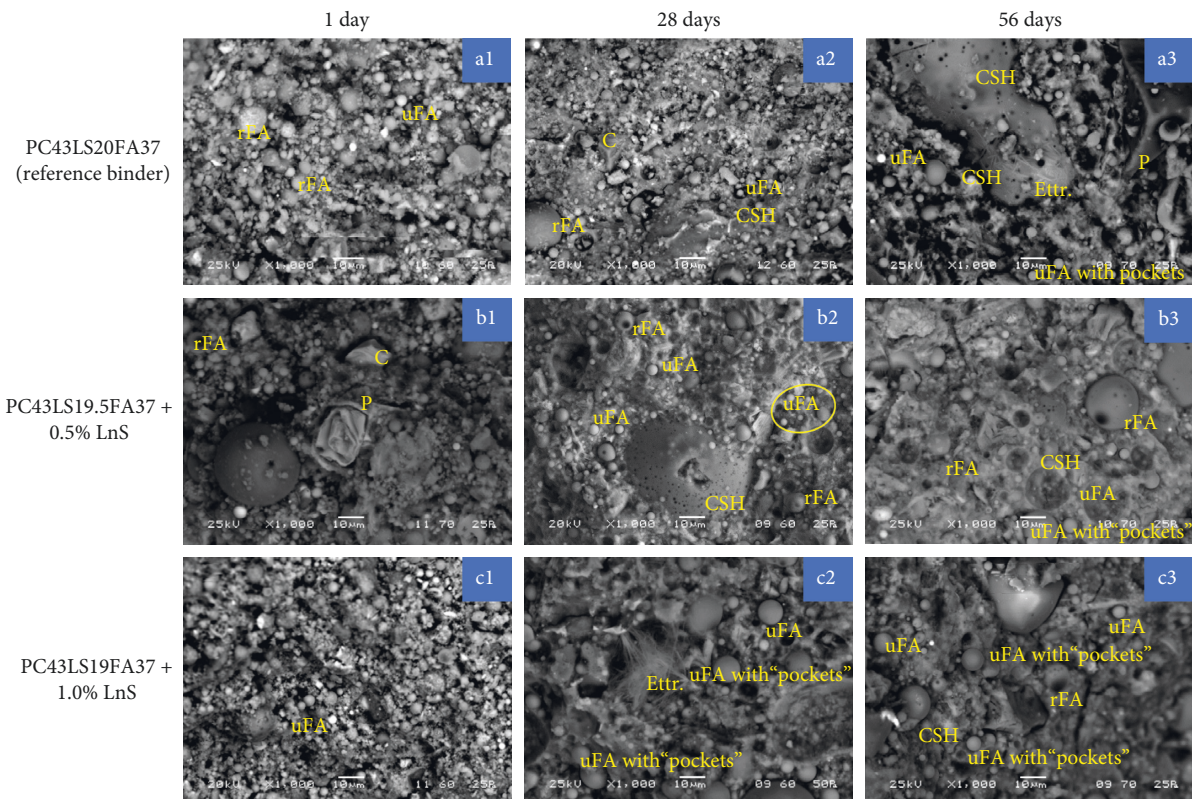

FIGURE 19: BSC micrograph of PC43LS20FA37 at low magnification at (a1) 1 day, (a2) 28 days, and (a3) 56 days; PC43LS19.5FA37 + 0.5% LnS at (b1) 1 day, (b2) 28 days, and (b3) 56 days; and PC43LS19FA37 + 1% LnS at (c1) 1 day, (c2) 28 days, and (c3) 56 days.

(ii) Prevalent reacted and unreacted FA particles and Ca(OH)$_2$ crystals exist.

(iii) Extended patches of dense areas of C–S–H can be distinguished.

Lastly, PC43LS19FA37 + 1% LnS bore resemblance to the optimal binder in terms of hydration products, morphology, and pozzolanic activity of the constituents. Qualitative differences were difficult to be identified by SEM,

however, more unreacted FA particles with dense rims surrounding them were spotted.

4. Conclusions

In this paper, a literature review was presented on recent research on the temperature ranges in which hydrates of nanocomposites decompose. Sixteen different novel cementitious nanocomposite binders were compared with two different reference binders, forming quaternary (PC, LS, FA, and nS) and quinary (PC, LS, FA, μS, and nS) combinations. The mechanical performance was determined in terms of cylinder compressive strength. The evolution of strength gain was described in a chronological scenario, and the thermal performance was assessed by thermal gravimetric analyses. Crystallographic and microstructural characteristics were also compared with the help of XRD and SEM, respectively. The following main outcomes can be drawn from the experimental results presented:

(i) TGA can be used to assess the pozzolanic activity of nanocomposite binders comprising of PC, LS, FA, nS, and/or μS, offering an approximation of the C–S–H produced

(ii) The clinker in cementitious binders can be lowered beyond the currently permissible limits set by the EU standards, with the use of nanoparticles of silica, which can deliver superior compressive strength and thermal and microstructural enhancement

(iii) The dispersion medium of nanoparticles in aqueous suspensions plays a significant role in the performance of the binders, and aqueous suspensions seem to exhibit a more predictable behaviour

(iv) Nanosilica competes with fly ash and silica fume, delaying pozzolanic reactions

(v) XRD confirmed the production of additional C-S-H from day 1 and the absence of carboaluminate hydrates

(vi) The direct correlation of microscopic results of $Ca(OH)_2$ content with macroscale results of compressive strength tests was verified in all quaternary and quinary formulations

(vii) Densification and microcracks reduction with nS content and age advancement were observed via SEM imaging.

(viii) Unreacted FA particles were found to be surrounded by "pockets" of hydrates not allowing them to participate in the pozzolanic reactions until the pH was elevated at later ages, and dense areas of what seems to be C–S–H (denoted by CSH on the micrographs) were also distinguished

(ix) As a conclusion, the optimal dosage was determined to be 0.5% nS by mass of the binder.

Data Availability

The data used to support the findings of this study (all excel data sheets with results) are included within the article.

Conflicts of Interest

The authors declare that they have no conflicts of interest.

Acknowledgments

References

[1] BSI, *BS EN 197-1:2011: Cement Part 1: Composition, Specifications and Conformity Criteria for Common Cements*, BSI, London UK, 2011.

[2] M. S. Meddah, M. C. Lmbachiya, and R. K. Dhir, "Potential use of binary and composite limestone cements in concrete production," *Construction and Building Materials*, vol. 58, pp. 193–205, 2014.

[3] A. Heath, K. Paine, S. Goodhew, M. Ramage, and M. Lawrence, "The potential for using geopolymer concrete in the UK," *Proceedings of the Institution of Civil Engineers-Construction Materials*, vol. 166, no. 4, pp. 195–203, 2013.

[4] G. Xu and X. Shi, "Characteristics and applications of fly ash as a sustainable construction material: a state-of-the-art review," *Resources, Conservation and Recycling*, vol. 136, pp. 95–109, 2018.

[5] K. Wang, S. P. Shah, N. Garg, G. Lomboy, S. Kawashima, and P. Hou, "Increasing use of fly ash in concrete through nanomaterial modification, multiscale characterization , and improved processing," ORAU-TVA Research Project Report (Grant No. 7-22976), 2013, http://152.87.4.98/kingston/reports_papers_presentations/pdf/465_TVA_Final_Report-Grant7-22976.pdf.

[6] A. M. Rashad, "A comprehensive overview about the effect of nano-SiO$_2$ on some properties of traditional cementitious materials and alkali-activated fly ash," *Construction and Building Materials*, vol. 52, pp. 437–464, 2014.

[7] S. Papatzani, K. Paine, and J. Calabria-Holley, "The effect of the addition of nanoparticles of silica on the strength and microstructure of blended Portland cement pastes," in *Proceedings of the International Concrete Sustainability Conference*, May 2014, http://www.nrmcaevents.org/?nav=display&file=648.

[8] С. Шаʃатзани, К. Пэйн, and Д. Калабрия-Чолли, "SiO$_2$ strength and microstructure of colloidal nanosilica enhanced cement pastes," *Cement and Its Application*, vol. 4, pp. 80–85, 2014, in Russian, http://www.cemcom.ru/2014_4%0D.

[9] S. Papatzani and K. Paine, "Lowering cement clinker: a thorough, performance based study on the use of nanoparticles of SiO$_2$ or montmorillonite in Portland limestone nanocomposites," *The European Physical Journal Plus*, vol. 133, no. 10, p. 430, 2018.

[10] S. Papatzani and K. Paine, "Polycarboxylate/nanosilica-modified quaternary cement formulations—enhancements and limitations," *Advances in Cement Research*, vol. 30, no. 6, pp. 256–269, 2018.

[11] D. Kong, Y. Su, X. Du, Y. Yang, S. Wei, and S. P. Shah, "Influence of nano-silica agglomeration on fresh properties of

cement pastes," *Construction and Building Materials*, vol. 43, pp. 557–562, 2013.

[12] M. Berra, F. Carassiti, T. Mangialardi, A. E. Paolini, and M. Sebastiani, "Effects of nanosilica addition on workability and compressive strength of Portland cement pastes," *Construction and Building Materials*, vol. 35, pp. 666–675, 2012.

[13] M. J. DeJong and F.-J. Ulm, "The nanogranular behavior of C–S–H at elevated temperatures (up to 700°C)," *Cement and Concrete Research*, vol. 37, no. 1, pp. 1–12, 2007.

[14] K. L. Scrivener, T. Füllmann, E. Gallucci, G. Walenta, and E. Bermejo, "Quantitative study of Portland cement hydration by X-ray diffraction/rietveld analysis and independent methods," *Cement and Concrete Research*, vol. 34, no. 9, pp. 1541–1547, 2004.

[15] T. D. Dyer, J. E. Halliday, and R. K. Dhir, "An investigation of the hydration chemistry of ternary blends containing cement kiln dust," *Journal of Materials Science*, vol. 34, no. 20, pp. 4975–4983, 1999.

[16] S. Kawashima, P. Hou, D. J. Corr, and S. P. Shah, "Modification of cement-based materials with nanoparticles," *Cement and Concrete Composites*, vol. 36, pp. 8–15, 2013.

[17] P. Hou, S. Kawashima, D. Kong, D. J. Corr, J. Qian, and S. P. Shah, "Modification effects of colloidal nanoSiO$_2$ on cement hydration and its gel property," *Composites Part B: Engineering*, vol. 45, no. 1, pp. 440–448, 2013.

[18] N. Farzadnia, A. A. Abang Ali, R. Demirboga, and M. P. Anwar, "Effect of halloysite nanoclay on mechanical properties, thermal behavior and microstructure of cement mortars," *Cement and Concrete Research*, vol. 48, pp. 97–104, 2013.

[19] F. Soleymani, "Optimum content of SiO$_2$ nanoparticles in concrete specimens," *Journal of American Science*, vol. 8, pp. 432–437, 2012, http://www.americanscience.org.

[20] S. F. Al-Otaibi, "Influence of nano-SiO$_2$ on the properties of cement pastes," in *Proceedings of the 4th International Symposium on Nanotechnology in Construction (NICOM)*, Crete, Greece, May 2012.

[21] S. Lim, P. Mondal, and I. Cohn, "Effects of incorporating nanosilica on carbonation of cement paste," *Journal of Materials Science*, vol. 50, no. 10, pp. 3531–3540, 2015.

[22] A. Nazari and S. Riahi, "Microstructural, thermal, physical and mechanical behavior of the self compacting concrete containing SiO$_2$ nanoparticles," *Materials Science and Engineering: A*, vol. 527, no. 29-30, pp. 7663–7672, 2010.

[23] L. Senff, D. Hotza, W. L. Repette, V. M. Ferreira, and J. A. Labrincha, "Effect of nanosilica and microsilica on microstructure and hardened properties of cement pastes and mortars," *Advances in Applied Ceramics*, vol. 109, no. 2, pp. 104–110, 2010.

[24] M. S. Morsy, S. H. Alsayed, and M. Aqel, "Effect of nano-clay on mechanical properties and microstructure of ordinary Portland cement mortar," *International Journal of Civil & Environmental Engineering IJCEE-IJENS*, vol. 10, no. 1, pp. 23–27, 2009.

[25] T.-P. Chang, J.-Y. Shih, K.-M. Yang, and T.-C. Hsiao, "Material properties of Portland cement paste with nano-montmorillonite," *Journal of Materials Science*, vol. 42, no. 17, pp. 7478–7487, 2007.

[26] W.-Y. Kuo, J.-S. Huang, and C.-H. Lin, "Effects of organo-modified montmorillonite on strengths and permeability of cement mortars," *Cement and Concrete Research*, vol. 36, no. 5, pp. 886–895, 2006.

[27] R. Yu, P. Spiesz, and H. J. H. Brouwers, "Effect of nano-silica on the hydration and microstructure development of ultra-high performance concrete (UHPC) with a low binder amount," *Construction and Building Materials*, vol. 65, pp. 140–150, 2014.

[28] Z. Rong, W. Sun, H. Xiao, and G. Jiang, "Effects of nano-SiO$_2$ particles on the mechanical and microstructural properties of ultra-high performance cementitious composites," *Cement and Concrete Composites*, vol. 56, pp. 25–31, 2015.

[29] F. T. Isfahani, E. Redaelli, F. Lollini, W. Li, and L. Bertolini, "Effects of nanosilica on compressive strength and durability properties of concrete with different water to binder ratios," *Advances in Materials Science and Engineering*, vol. 2016, Article ID 8453567, 16 pages, 2016.

[30] L. P. Singh, D. Ali, and U. Sharma, "Studies on optimization of silica nanoparticles dosage in cementitious system," *Cement and Concrete Composites*, vol. 70, pp. 60–68, 2016.

[31] S. Papatzani, "Effect of nanosilica and montmorillonite nanoclay particles on cement hydration and microstructure," *Materials Science and Technology*, vol. 32, no. 2, pp. 138–153, 2016.

[32] S. Papatzani and K. Paine, "Dispersed inorganic or organo-modified montmorillonite clay nanoparticles for blended Portland cement pastes: effects on microstructure and strength," in *Nanotechnology in Construction*, K. Sobolev and S. P. Shah, Eds., pp. 131–139, Springer International Publishing, Cham, Switzerland, 2015.

[33] S. Papatzani, E. G. Badogiannis, and K. Paine, "The pozzolanic properties of inorganic and organomodified nano-montmorillonite dispersions," *Construction and Building Materials*, vol. 167, pp. 299–316, 2018.

[34] J. Čėsnienė, A. Baltušnikas, I. Lukošiūtė, K. Brinkienė, and R. Kalpokaitė-Dičkuvienė, "Influence of organoclay structural characteristics on properties and hydration of cement pastes," *Construction and Building Materials*, vol. 166, pp. 59–71, 2018.

[35] M. Monasterio, J. J. Gaitero, E. Erkizia et al., "Effect of addition of silica- and amine functionalized silica-nanoparticles on the microstructure of calcium silicate hydrate (C–S–H) gel," *Journal of Colloid and Interface Science*, vol. 450, pp. 109–118, 2015.

[36] J. Calabria-Holley, K. Paine, and S. Papatzani, "Effects of nanosilica on the calcium silicate hydrates in Portland cement-fly ash systems," *Advances in Cement Research*, vol. 27, no. 4, pp. 187–200, 2015.

[37] J. Zhang and G. W. Scherer, "Comparison of methods for arresting hydration of cement," *Cement and Concrete Research*, vol. 41, no. 10, pp. 1024–1036, 2011.

[38] G. Bye, P. Livesey, and L. Struble, *Portland Cement*, ICE Publishing, 2007, https://www.icebookshop.com/Products/Portland-Cement,-3rd-edition.aspx.

[39] J. Calabria-Holley, K. Paine, and S. Papatzani, "Effects of nanosilica on the calcium silicate hydrates in Portland cement-fly ash systems," *Advances in Cement Research*, vol. 27, no. 4, pp. 187–200, 2014.

[40] R. F. Feldman, G. G. Carette, and V. M. Malhotra, "Studies on mechanics of development of physical and mechanical properties of high-volume fly ash-cement pastes," *Cement and Concrete Composites*, vol. 12, no. 4, pp. 245–251, 1990.

[41] S. Gupta, "Application of silica fume and nanosilica in cement and concrete—a review," *Journal on Today's Ideas-Tomorrow's Technologies*, vol. 1, no. 2, pp. 85–98, 2014.

[42] K. De Weerdt, K. O. Kjellsen, E. Sellevold, and H. Justnes, "Synergy between fly ash and limestone powder in ternary

cements," *Cement and Concrete Composites*, vol. 33, no. 1, pp. 30–38, 2011.

[43] L. Lam, Y. L. Wong, and C. S. Poon, "Degree of hydration and gel/space ratio of high-volume fly ash/cement systems," *Cement and Concrete Research*, vol. 30, no. 5, pp. 747–756, 2000.

[44] P. Hosseini, R. Hosseinpourpia, A. Pajum, M. M. Khodavirdi, H. Izadi, and A. Vaezi, "Effect of nano-particles and aminosilane interaction on the performances of cement-based composites: an experimental study," *Construction and Building Materials*, vol. 66, pp. 113–124, 2014.

[45] S. Papatzani, K. Paine, and J. Calabria-Holley, "A comprehensive review of the models on the nanostructure of calcium silicate hydrates," *Construction and Building Materials*, vol. 74, pp. 219–234, 2015.

[46] K. De Weerdt, M. B. Haha, G. Le Saout, K. O. Kjellsen, H. Justnes, and B. Lothenbach, "Hydration mechanisms of ternary Portland cements containing limestone powder and fly ash," *Cement and Concrete Research*, vol. 41, no. 3, pp. 279–291, 2011.